An intelligent structural damage detection approach based on self-powered wireless sensor data

Article *in* Automation in Construction · February 2016

DOI: 10.1016/j.autcon.2015.10.001

5 authors, including:

Amir H. Alavi
University of Pittsburgh
208 PUBLICATIONS **10,816** CITATIONS
SEE PROFILE

Hassene Hasni
Michigan State University
35 PUBLICATIONS **533** CITATIONS
SEE PROFILE

Karim Chatti
Michigan State University
122 PUBLICATIONS **1,164** CITATIONS
SEE PROFILE

Fred Faridazar
U.S. Department of Transportation
11 PUBLICATIONS **218** CITATIONS
SEE PROFILE

An Intelligent Structural Damage Detection Approach Based on Self-Powered Wireless Sensor Data

Amir H. Alavi[1], Hassene Hasni, Nizar Lajnef, Karim Chatti

Department of Civil and Environmental Engineering, Michigan State University, East Lansing, MI 48823, USA.

&

Fred Faridazar

Federal Highway Administration, Turner-Fairbank Highway Research Center, McLean, VA, USA.

This study presents the results of an ongoing research project conducted by the U.S. Federal Highway Administration (FHWA) on developing an intelligent approach for structural damage detection. The proposed approach is established upon the simulation of the compressed data stored in memory chips of a newly developed self-powered wireless sensor. An innovative data interpretation system integrating finite element method (FEM) and probabilistic neural network (PNN) based on Bayesian decision theory is developed for damage detection. Several features extracted from the cumulative limited static strain data are used as damage indicator variables. Another contribution of this paper is to define indicator variables that simultaneously take into account the effect of array of sensors. The performance of the proposed approach is first evaluated for the case of a simply supported beam under three-point bending. Then, the efficiency of the method is tested for the complicated case of a bridge gusset plate. The beam and gusset plate structures are analyzed as 3D FE models. The static strain data from the FE simulations for different damage scenarios is used to calibrate the sensor-specific data interpretation algorithm. The viability and repeatability of the method is demonstrated by conducting a number of simulations. Furthermore, a general scheme is presented for finding the optimal number of data acquisition points (sensors) on the structure and the associated optimal locations. An uncertainty analysis is performed through the contamination of the damage indicator features with different Gaussian noise levels.

Keywords: Structural Health Monitoring; Self-Powered Wireless Sensor; Damage detection; Uncertainty analysis; Probabilistic neural networks

[1] Corresponding author:
E-mail: alavi@msu.edu, ah_alavi@hotmail.com

1. Introduction

Structural health monitoring (SHM) is an emerging field in civil engineering for continuous damage assessment and safety evaluation of infrastructures. As a result of notable developments in the signal analysis and information processing techniques, numerous structural damage identification approaches are developed [1-4]. In this context, one of the most widely-used approaches is vibration-based method [5,6]. Signal and model-based techniques are the main classes of the vibration-based method. The first category is based on defining the damage by indices and comparing the structural responses before and after damage [7-9]. The signal-based methods are generally appropriate for detecting the damage locations [3]. On the other hand, a major feature of the model-based methods is that they can detect both the damage locations and severities by improving the structural mathematical model [10-13]. An advantage of using such methods is that they require a relatively small number of sensors. Furthermore, they are highly effective for monitoring catastrophic events. However, a notable limitation of these techniques is that they are not sufficiently sensitive for detecting long term minor fatigue damage. A comprehensive review about the existing structural damage detection techniques can be found in [14-17]. Another class of the damage detection methods, called nondestructive evaluation (NDE) or nondestructive inspection has been the focus of many studies. NDE is the structural condition assessment without removing the individual structural components [18-20]. The NDE technology is commonly classified as a local-based damage detection approach. Some of the well-known NDE techniques are acoustics, emission spectroscopy, fiber-optic sensors, fiber-scope, hardness testing, leak testing, magnetic perturbation, X-ray, pulse-echo, and radiography [18].

In the last decade, significant attention has been devoted to the utilization of new sensing technologies for instrumentation within the structural systems. A major drawback of using traditional wired sensors pertains to the difficulties in deploying and maintaining the associated wiring system. Moreover, managing huge amount of data generated by a dense array of wired sensors is very challenging and costly [21]. To cope with these limitations, wireless sensor

networks (WSNs) are increasingly utilized as alternatives to traditional structural engineering monitoring systems. The significant capability of WSNs for sensing the physical state of the structural systems has attracted considerable attention in recent years [22-30]. In addition to the conventional monitoring applications of WSNs, they are autonomous data acquisition nodes providing valuable spatio-temporal information of the structure [31-35]. Dense arrays of low-cost smart wireless sensors can offer useful data about the structural deterioration. Such information can be efficiently used to enhance the performance of the SHM systems [21]. Recent development and applications of smart sensors and sensing systems are comprehensively introduced by Sundaram et al. [21] and Yun and Min [36]. However, a major concern for the application of wireless sensors is related to the difficulties of powering them. To tackle this issue, harvesting ambient energy seems to be an attractive solution [37-49]. Energy harvesting is the possibility of converting mechanical energy into electrical energy [50]. Among various self-powering energy sources, piezoelectric transducers are proved to be one of the most efficient choices [21-53]. For SHM, piezoelectric transducers can be used for the self-powering of wireless sensors through harvesting energy from the mechanical loading experienced by the structure [54]. Recently, a new class of self-powered wireless sensors has been developed by the authors at Michigan State University (MSU) based on "smart" pebble concept [52-55]. The "smart" pebble generally refers to a battery-less sensor having a size comparable to the grain size of the construction material. By embedding these sensors inside the structure, it is possible to monitor the localized strain statistics. The recorded information can be used for early damage detection and future condition evaluation. Research in the previous FHWA funded project revealed the applicability of the MSU's smart pebble self-powered wireless sensor (SWS) for continuous monitoring of pavement structures [51-55]. This unique sensor is based on the integration of piezoelectric transducers with an array of ultra-low power floating gate computational circuits [53]. A series of memory cells store the load history profiles that are transferred to the data logger system as a voltage signal through the piezoelectric effect. Each of the memory cells records events at a specific preset level. The output is reported in the form of a

histogram where each bin represents the cumulative time of occurrences at a predetermined load level. Despite several advantages of using SWS, there would be a considerable loss of information. In fact, a part of the sensed information is compressed as a function of cumulative time at each load level. This drawback results in a notable difficulty in the interpretation of the data generated by SWS [39, 54]. There are some statistical and probabilistic methods to generate full-field data based on the information from existing wireless sensor data. Some examples are smoothing element analysis and inverse FE method [56], listwise and pairwise data deletion, mean substitution, and expectation maximization [57, 58]. Recently, Lajnef et al. [54] developed a method for predicting remaining fatigue life of pavement using the data provided by SWS. Moreover, they used a classical statistical technique, called ordinary Kriging to generate the missing data from a set of measurements by SWS. Also, SWS has been successfully used for the long-term fatigue monitoring in biomechanical implants [53].

This study presents a new methodology for the structural damage detection based on the simulation of the SWS data. The proposed approach uses features extracted from the cumulative time strain distributions at preselected discrete levels. In order to analyze the cumulative static strain data, a hybrid method of probabilistic neural network (PNN) and FE is proposed. PNN is a neural network implementation of the well-established Bayesian classifier method [58]. The FE models of a simply supported beam and a gusset plate with complex geometry components are used as representatives of the real structures for method verification. For the analysis, different damage scenarios are introduced to these structures. The resulting static strain data are used as feature vector for the damage detection process.

2. The Proposed Methodology

Damage detection algorithms are one of the main parts of the SHM systems. Such algorithms are developed to analyze raw sensor data and provide a precise diagnosis of the damage state. Apparently, quality and quantity of raw sensor data have a direct effect on the accuracy of damage detection [59]. As discussed before, the new SWS made at MSU is capable of

continuously monitoring of local strain events within the host structure [54]. Fig. 1 shows a full prototype of the current version of the sensor enclosed in an H-shape package.

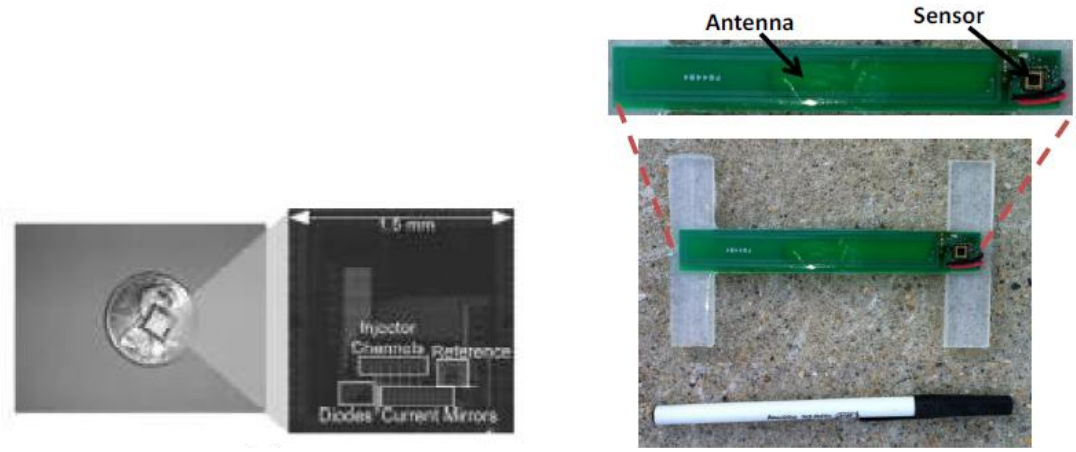

Fig. 1. Current version of the smart sensor enclosed in an H-shape package [39, 55, 60]

These sensors have a series of memory cells that cumulatively store the duration of strain events, at a preselected level discretization. They measure the duration of events when the amplitude of the input signal, coming from the piezoelectric, exceeds different thresholds. Fig. 2 presents a schematic representation of the level crossing cumulative time counting implemented by the developed SWS.

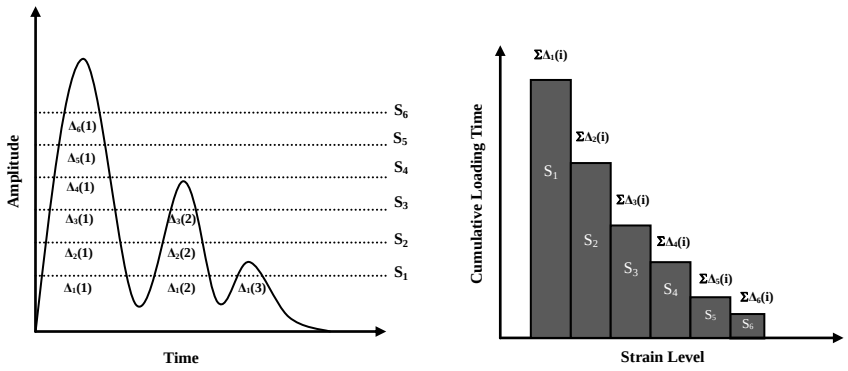

Fig. 2. The level crossing cumulative time counting implemented by a self-powered wireless sensor

As can be observed from Fig. 2, the only information that can be extracted from the sensor is the cumulative duration of strain events. Accordingly, the sensor does not provide information about

the normally distributed strain histograms induced by the service loads every reading period. That is why interpreting the data generated by SWS is a complicated task and highly desired. In order to develop a damage detection algorithm based on the simulation of such limited data, a new approach is considered in this research. It is well-known that the service load in structures is usually defined by a Gaussian distribution and thus the induced local strain. With a Gaussian distributed load, the sensor output is the summation of the cumulative time strain distributions. Since the summation of Gaussian distributions can be assumed by a Gaussian distribution, this study rationally assumes that the sensor output can be characterized by the following cumulative density function (CDF):

$$F(\varepsilon) = \frac{\alpha}{2}\left[1 - erf\left(\frac{\varepsilon-\mu}{\sigma\sqrt{2}}\right)\right] \quad (1)$$

where

μ: Mean of the strain distribution

σ: Standard deviation that account for the load and frequency variability

α: Total cumulative time of the applied strain.

On the basis of previous research [54], μ and σ of the cumulative time distribution can be regarded as good indicators of the damage progression. In fact, μ and σ are the only viable tools to define the SWS output data. These parameters can be obtained by a curve fitting of the sensor output distribution collected from the entire memory cells. Consequently, the damage state can be logically considered to be a function of μ and σ. The other influencing input parameter included in the analysis is the sensor location. Obviously, damage detection process can be treated as a pattern recognition and classification problem. The solution is to use a classifier which can classify structures either as damaged or healthy. To this aim, a PNN-based damage state classification strategy is proposed. The study procedure includes the structural simulation with FEM for different damage scenarios, generation of calibration samples and pattern classification of testing samples. New features are defined that simultaneously take into account the effect of array of scattered sensors. This is mostly of importance for resolving the concerns

for installation procedure of sensors in the field, particularly for pavements. Since the method is capable of analyzing the data generated by the randomly distributed sensors, the pebble size SWS can be placed in the mix at the site or tossed into the paving materials during construction. Fig. 3 illustrates a flow chart of a damage pattern classification model. The μ and σ values are obtained through the fitting of a CDF (Eq. (1)) to the cumulative duration of strain events at each data acquisition point (sensor). These parameters are used as feature vectors for the calibration of the classifier. Thereafter, validation process is used to check the performance of the classifier. If convergence condition (desired accuracy) is satisfied, then the process is stopped and the optimal number of sensors is reported. Otherwise, the algorithm returns back to optimum sensor number selection process until the specified convergence condition is satisfied. The details of the procedure are fully described in the next section.

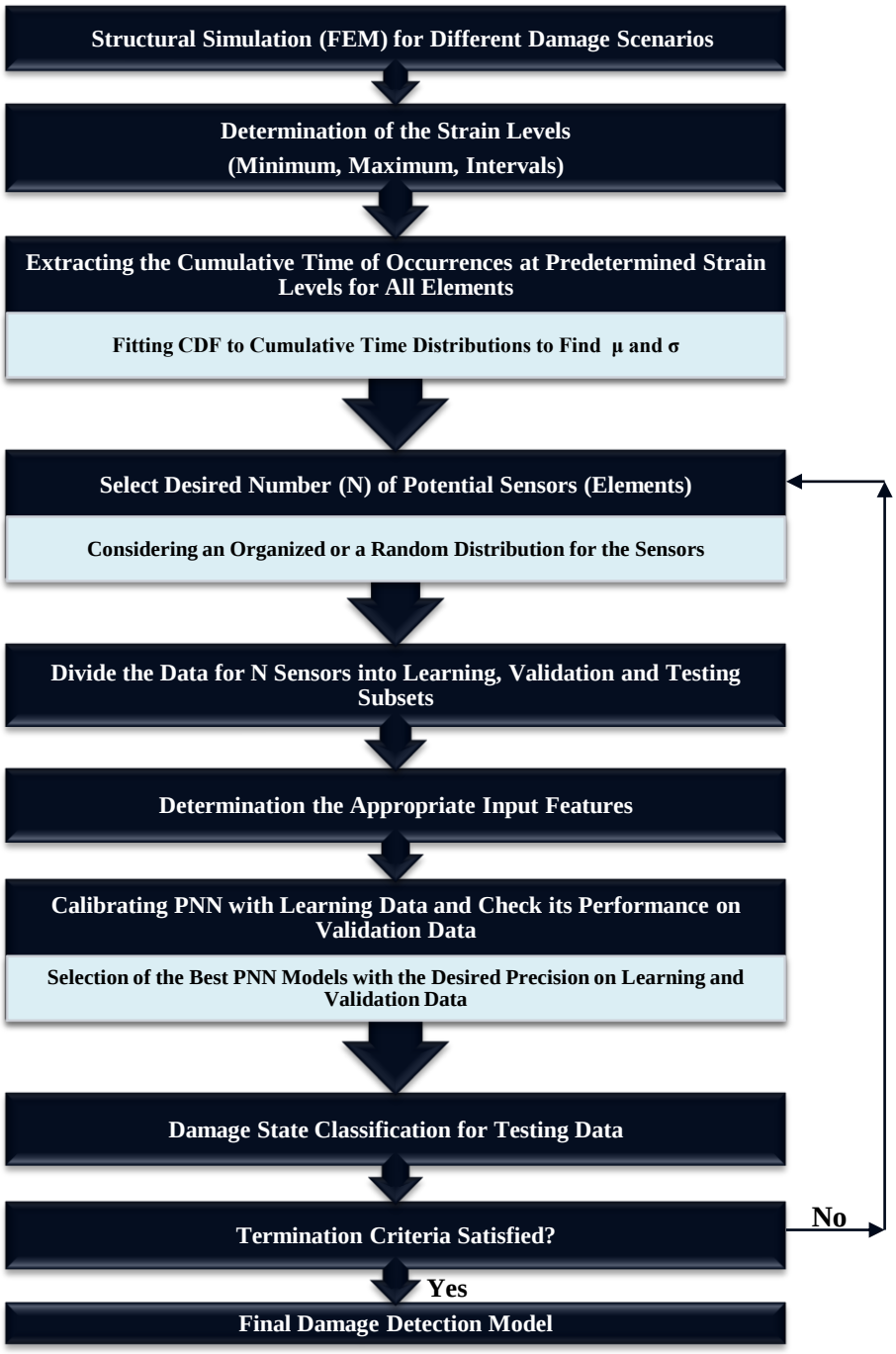

Fig. 3. Flow chart of the proposed damage pattern classification model

3. Performance Verification

The performance of the proposed methodology is verified in two stages. At the first stage, the method is applied to simply supported intact and damaged concrete beams under three-point bending. The second stage is focused on the verification of the method for a much more complicated case which is a bridge gusset plate. A series of FE simulations are conducted for both of the cases and the derived models are considered as representatives of the real structures.

Static strain measurements at specified or randomly selected locations are used to calibrate the supervised learning algorithm. Different techniques can be utilized to solve linear elastic fracture mechanics problems [51, 61]. However, the FE method is considered reliable because of its applicability to most elasticity problems, as well as its ease of implementation [51, 62, 63]. Herein, the structures under consideration are assumed to be linearly elastic and are analyzed as 3D FE models using Abaqus Version 6.12-3. In the FE simulations of beam, axial strains at the sensor locations are of interest. That is to say, only in-plane strains are considered to produce electric charge. For the gusset plate, maximum principle strains are used due to the complexity of the geometry. As a fairly similar loading pattern to real traffic load distribution, the input loading type is in the form of half-sine loading (Fig. 4). There are data acquisition points remote to the damage sites that will not be any influenced by the damage. Thus, in real conditions, the sensors will not record any information. To consider this issue in this study, the data for such as acquisition points are not included in the analyses. It is worth mentioning that main focus of this research is to propose a pioneering damage detection concept and then verify its performance for a simple case and then for a complicated structure, such as the gusset plate. Thus, the issue of controlling different mesh sizes, changing the material properties, loading, etc was not within the scope of this work.

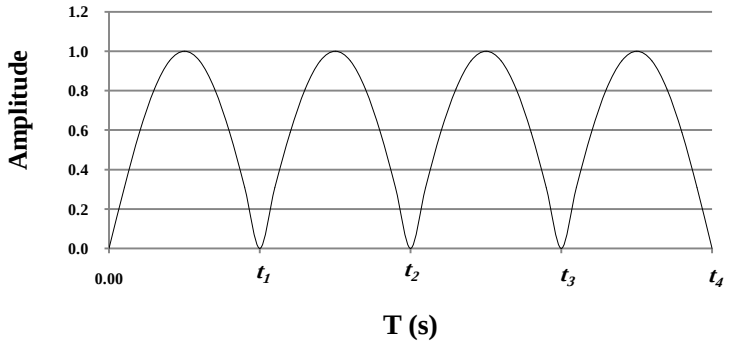

Fig. 4. The half-sine loading cycles

3.1. Case I: Simply Supported Beam

Fig. 5 shows the geometry and loading of the investigated beams. The beam is modeled using three dimensional eight node linear brick elements (C3D8R). For Case I, the sensor locations are assumed to be randomly distributed but not very close to the notch (crack). Thus, sophisticated modeling (meshing) of the notch is not required. The FE model and mesh are shown in Fig. 6. The model of intact beam consists of 158 C3D8R elements corresponding to 380 nodes. Taking into account the size of the real smart pebble sensors and also to facilitate the implantation of the algorithm, a fairly course meshing is considered. Thus, each of the elements of the FE model can be a possible sensor location. Alternatively, in case of applying a finer mesh, the averages of the strains at elements equivalent to the probable sensor volume can be used. It is assumed that the damaged zone extends through the entire width of the beam. The damage is simulated by removing rectangular sections of different sizes at the centre of the beam. In this model, uniform pressure load is applied on the top of the beam. The amplitude of the load is optimally taken in a way that there would be a sense of stress throughout the beam. However, the material and geometry properties used in the model are as given below.

- E = 29000MPa
- Poisson Ratio = 0.2
- Density = 2400 kg/m³
- Dimensions (L, D, W): 400×100×10mm
- Load (Pressure): 10 MPa
- Load Frequency = 2Hz

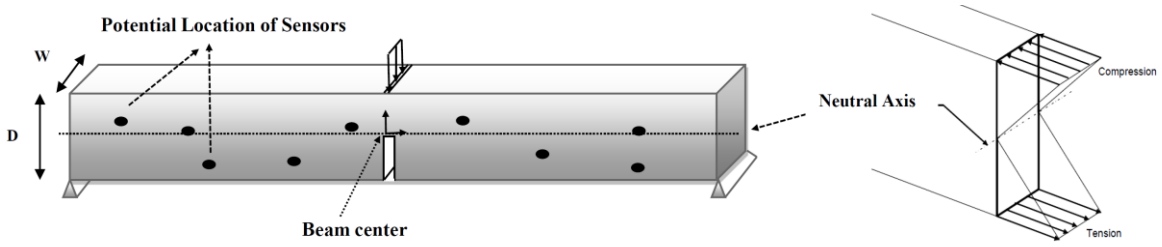

Fig. 5. Geometry and loading of a damaged simply supported concrete beam

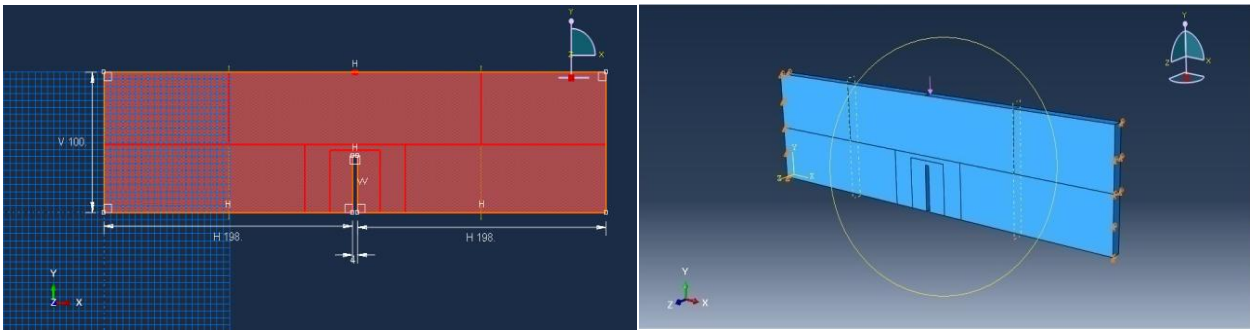

Fig. 6. The FE model of a simply supported beam

3.1.1. Data Processing

The FE model of the beam is used as a representation of the real structure. Static strain data of the surface nodes is extracted from the simulations and used to derive the feature vectors for the damage state classification process. To validate the efficiency of the proposed approach, different damage scenarios are considered. The severity of damage is defined by changing the notch to the beam depth (a/D) as follows:

1: Intact beam (a/D = 0.00)

2: a/D = 0.05

3: a/D = 0.1

4: a/D = 0.2

5: a/D = 0.3

6: a/D = 0.4

7: a/D = 0.45

The FE simulation results for some of the damage scenarios (i.e., Classes 1, 5, 7) are shown in Fig. 7. The presented results belong to the maximum loading step. As discussed before, SWS has a series of memory cells (gates). Each of these gates cumulatively stores the duration of strain events at a preselected levels. In general, the number of gates is dependent on the nature of the problem and the material. In this study, a typical number of 10 is considered for the strain levels to efficiently cover the lower and upper limits of the strain values extracted from the FE

simulations of seven damage scenarios. The minimum and maximum of the strain values are about 0.122 and 288.965 με, respectively. Thus, for the analysis, the lower and upper bounds of the strain levels are, respectively, set to 0.100 and 300.000 με. Ten gates are considered and therefore the difference between the strain levels is 33.322 με. The preselected strain levels are shown in Table 1. Using the strain histories of all elements, a script is written in MATLAB to perform the following tasks:

a) Takes the strain-time data from Abaqus and measures the duration of events at the strain levels defined in Table 1.
b) Fits CDF given in Eq. (1) to the cumulative time of occurrences at predetermined strain levels obtained from the first step.
c) Reports the μ and σ for the elements
d) Returns the horizontal and vertical distance of the sensor from the beam center

Fig. 8 illustrates a representative example of the above procedure for one of the elements. The obtained data are subsequently used to calibrate the PNN classifier.

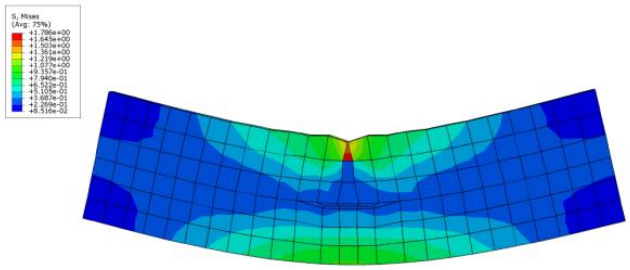

(a) Intact beam(Class 1: a/D= 0)

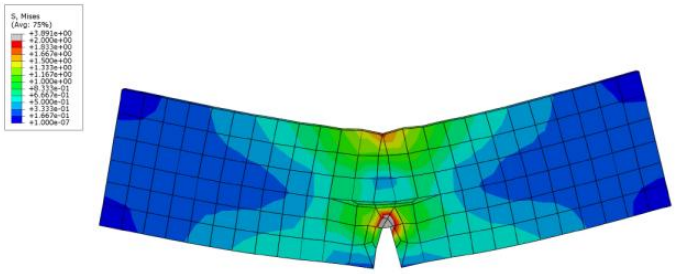

(b) Damaged beam (Class 5: a/D= 0.3)

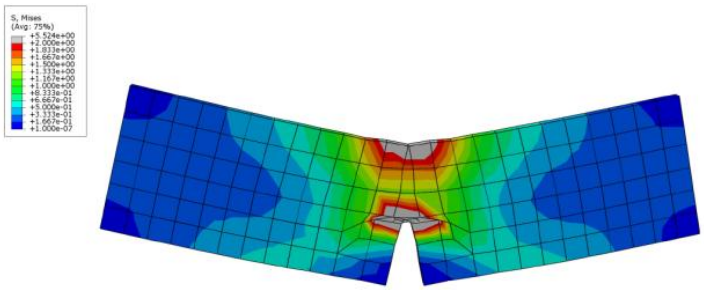

(c) Damaged beam (Class 7: a/D= 0.45)

Fig. 7. The FE simulation results for different damage scenarios for Case I (Von Mises stress distribution).

Table 1. The preselected strain levels considered for the analysis

Gate number	Strain Level (με)
1	0.100
2	33.422
3	66.744
4	100.067
5	133.389
6	166.711
7	200.033
8	233.356
9	266.678
10	300.000

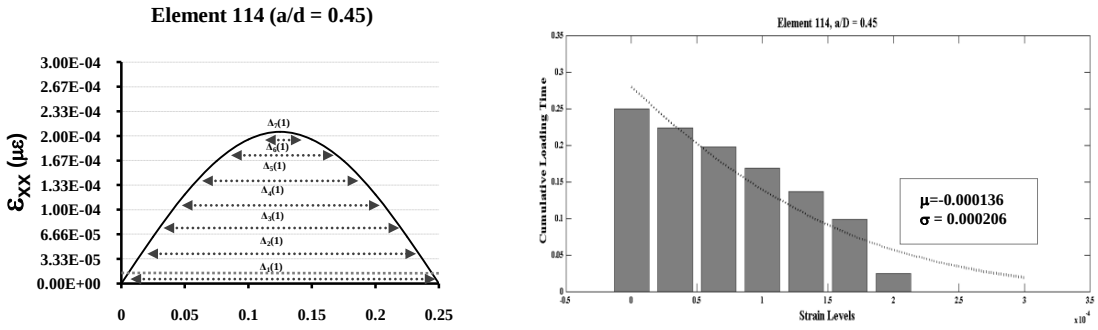

Fig. 8. A typical curve fitting of cumulative time of occurrences at predetermined strain levels

3.2. Case II: Gusset Plate of Bridge

In 2007, the deck truss portion of the I-35W Highway Bridge in Minneapolis, Minnesota collapsed. According to The National Transportation Safety Board [64], the collapse occurred due to a bending instability in the U10W gusset plates. Due to the importance of this catastrophic event, the failure analysis of the I-35W Highway Bridge has been the focus of many studies (e.g. [65-68]). In this study, a gusset plate with a structure similar but not exactly identical to that of the I-35W Highway Bridge is considered for further verification of the proposed approach. The 3D FE model for the gusset plate is shown in Fig. 9. The dimension of the joint is given in Fig. 10. Besides, Fig. 11 describes the location and the magnitude of the loading. The load magnitude is taken equal to 10% of the critical loading at the time of bridge collapse [66]. The plate is modeled using three dimensional linear tetrahedral elements (C3D4). The model of the gusset plate consists of about 50000 C3D4 elements corresponding to about 25000 nodes. However, the material and geometry properties used in the model are as given below.

- E = 200000MPa (Steel ASTM-A36)
- Poisson Ratio = 0.3
- Density = 7800 kg/m³
- Load Frequency = 0.5Hz

The thickness of the gusset plate is 0.5 inch (12.7 mm). The diameter for the data accusations nodes (potential sensors) is equal to 10 mm. The average of the max principle strains at the nodes within the sensor specified area is taken as the representative strain value for each sensor. Several sensors are considered for the analysis. The distance between the sensors is taken 80mm. Considering the dimension of the plate, 28 and 16 sensors are defined in the horizontal and vertical directions, respectively. Thus, the maximum number of data acquisitions nodes is 28 × 16 = 448. The location of sensors in the gusset plate can be seen in Fig. 9.

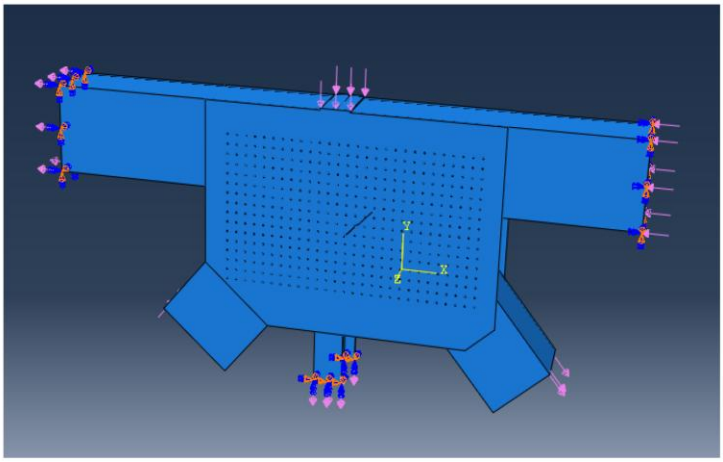

Fig. 9. The geometry of the gusset plate

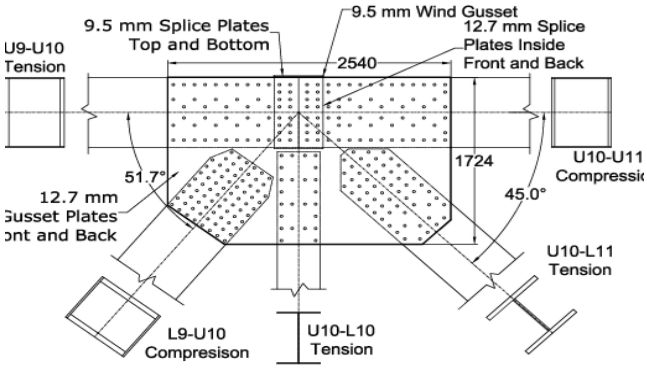

Fig. 10. Dimensions of the gusset plate joint [66]

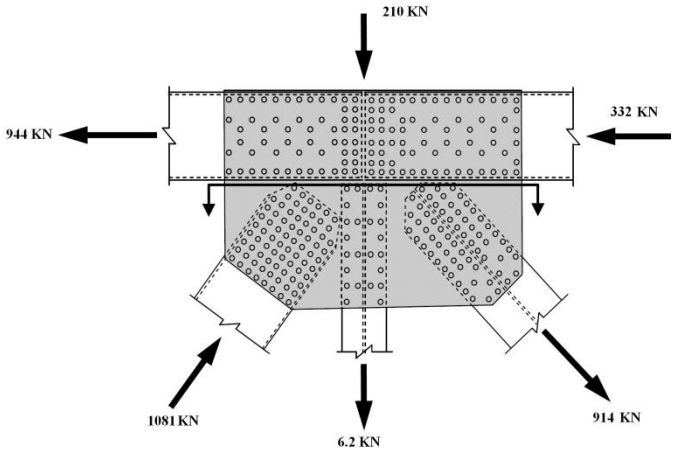

Fig. 11. The location and the magnitude of the loading

3.2.1. Data Processing

Similar to Case I, static strain data of the surface nodes extracted from the FE simulations are used for the damage detection. In order to have a more realistic definition of the damage progress, an extended finite element method (XFEM) analysis is first performed. XFEM is an efficient extension to classical FEM to model the propagation of various discontinuities such as cracks [69]. Herein, an XFEM crack with a small length (10 mm) is created at the middle of the plate and then the load is increased to capture the crack propagation status. Fig. 12 illustrates the results of the XFEM analysis for critical loading along with the crack propagation direction.

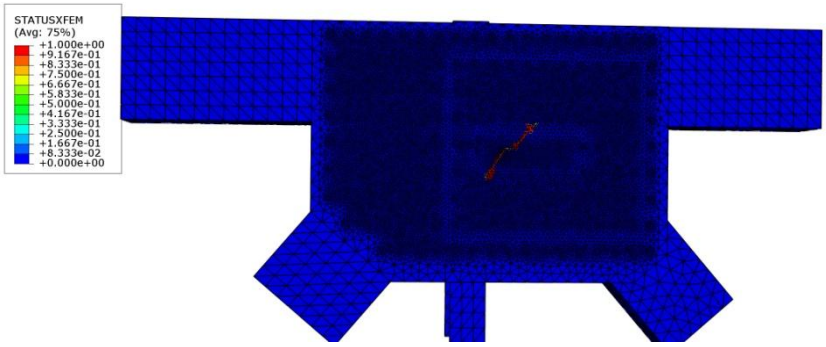

(a) Crack propagation direction

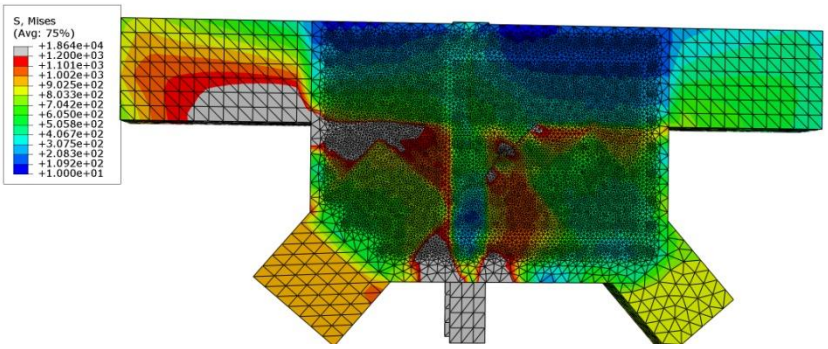

(b) Von Mises stress distribution for critical loading

Fig. 12. The results of the XFEM analysis

Taking into account the final length of the crack at the plate failure (530 mm) and its direction, fifteen damage states (classes) are defined. The damage is simulated by creating notches of different sizes through a new series of FE analyses. Fig. 13 presents a schematic definition of different damage states for the gusset plate. The first damaged case belongs to the initial notch

with 10 mm length. The other states are created by adding 20 mm to each side of the initial notch on the direction already detected by XFEM. For instance, the third damaged class pertains to the notch with an initial length of 10 mm plus 20 mm on each side, 10 + 20 + 20 = 60 mm. Subsequently, the damage classes can be defined by changing the notch size (a) as follows:

1: Intact beam (a= 0 mm)

2: a = 10 mm (Initial notch)

3: a = 50 mm

4: a = 90 mm

5: a = 130 mm

6: a = 170 mm

7: a = 210 mm

8: a = 250 mm

9: a = 290 mm

10: a = 330 mm

11: a = 370 mm

12: a = 410 mm

13: a = 450 mm

14: a = 490 mm

15: a = 530 mm

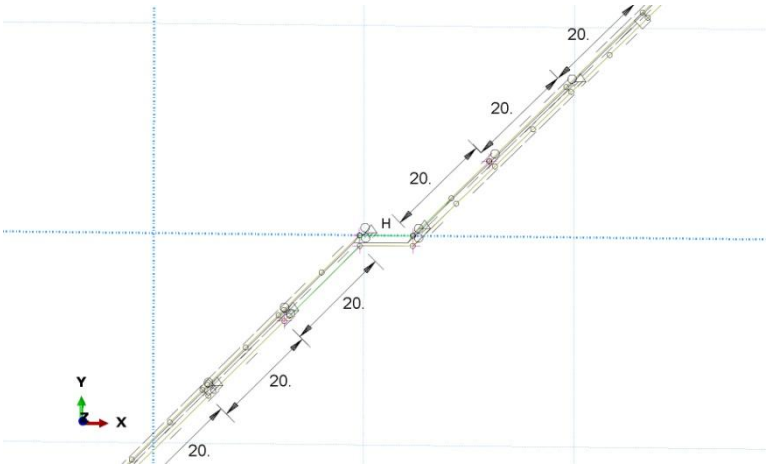

Fig. 13. Definition of different damage states for the gusset plate

The FE simulation results for some of the damage scenarios (i.e., Classes 1, 7, 9) are shown in Fig. 14. Since Case II, is a realistic case, the number of gates (strain levels) is selected according to the piezoelectric properties considered for the design of the smart pebble sensors. The minimum level of strains to be captured by piezoelectric transducers is about 30.00 με. On the other hand, the maximum of the strain value extracted from the FE simulations of fifteen damage scenarios is about 150 με. Considering a reasonable number of ten strain levels for the gates, the difference between the strain levels is 13.33 με. Table 2 presents the preselected strain levels for the gusset plate. The MATLAB script written for Case II performs all the tasks that are described for Case I. Additionally, for this complicated case, the new script takes the strain-time data from Abaqus and finds the strain information for the considered 448 or any other number of sensors with different sizes (for this case: 10 mm).

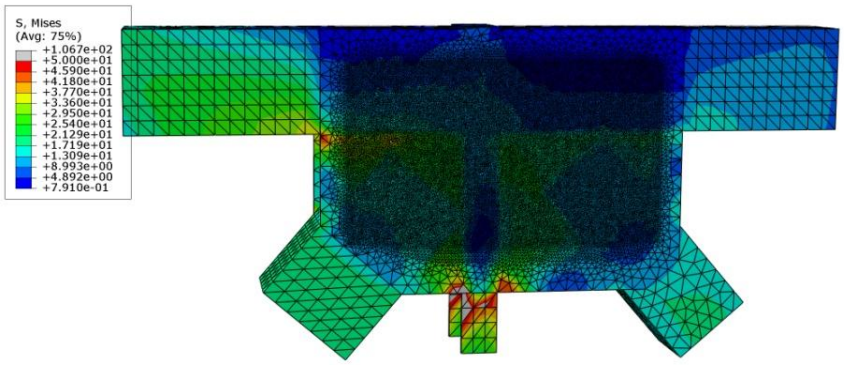

(a) Intact plate (Class 1: a = 0 mm)

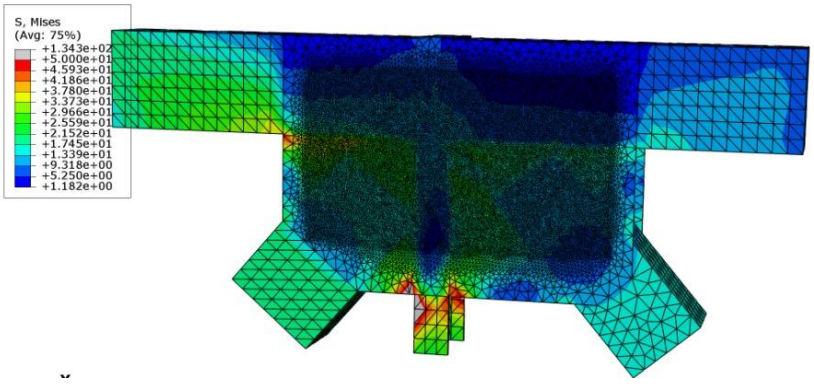

(b) Damaged plate (Class 7: a = 200 mm)

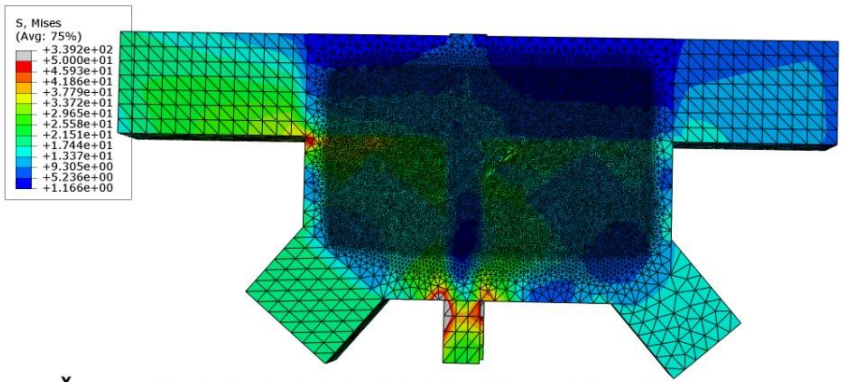

(c) Damaged plate (Class 9: a = 280 mm)

Fig. 14. The FE simulation results for typical damage scenarios for Case II (Von Mises stress distribution).

Table 2. The preselected strain levels considered for the analysis

Gate number	Strain Level (με)
1	30.00
2	43.33
3	56.67
4	70.00
5	83.33
6	96.67
7	110.00
8	123.33
9	136.67
10	150.00

4. Implementation and Simulation Results

As discussed before, each of the nodes and elements of the FE models can be a possible sensor location. In order to perform the damage analysis, different numbers of data acquisition nodes are considered as potential sensors. The first stage is a basic analysis focused on detecting the damage introduced to the simply supported beam. Thereafter, the findings from this important stage are used to detect the damage states defined for the realistic gusset plate case. For the beam case, each of the elements represents a sensor location. For the gusset pate with complex

meshing, the diameter for the potential sensors is equal to 10 mm. Although the main goal is to provide good damage detection accuracy, the nature of the simulations provides a chance of evaluating the optimal number of sensors required for a precise damage detection. The performance of the models developed for each sensor configuration is measured using the Detection Rate (DR) defined as follows:

$$DR = \frac{Number\ \ of\ Damage\ \ States\ \ Correctly\ \ Classified}{Total\ \ Number\ \ of\ Data\ Sets\ in\ Configuration} \quad (2)$$

In the following sections, the details of the PNN algorithm used for the damage state classification are described. Subsequently, comprehensive explanations about the implementation of the method and the simulation results are provided.

4.1. Probabilistic Neural Network

Computational intelligence (CI) techniques are considered as alternatives to existing traditional methods for tackling real world problems. They determine the model structure by automatically learning from data. CI has different well-known branches such as artificial neural network (ANN), fuzzy inference system (FIS), adaptive neuro-fuzzy system (ANFIS), and support vector machines (SVM). These techniques have been successfully employed to solve a variety of problems in engineering field [70-94]. Among different CI techniques, ANNs have been widely used in the field of damage detection and structural identification [95-105]. A major drawback of the conventional ANNs pertains to the time-consuming iterative procedure required during training of the network to obtain the optimal learning parameters [106]. To overcome such limitation, PNN has been proposed by Specht [107]. PNN is essentially based on the well-known Bayesian classification by combining the Bayes strategy for decision making with a non-parametric estimator for the probability density functions (PDFs). It can be used for direct estimation of posterior probability densities and pattern classification [58]. There are some studies in the literature focusing on the application of PNN to the structural damage identification (e.g., [108-113]). Some of the advantages of PNN over the conventional ANN are

[114]: (i) The PNN execution is generally much faster than the conventional neural network because it does not require a separate training phase, (ii) Training of the PNN algorithm with new training data is fairly easy, and (iii) This method provides good classification performance in domains with noisy data. Despite significant capabilities of PNN, its application to the interpretation of the data generated by WSN or SWS is totally new and original.

The PNN algorithm adopts a Bayes decision rule, i.e. it considers a test vector x with m dimensions that belongs to one of the classes $C_1, C_2, \ldots, C_k$. From the multi-category classifier decision, x belongs to C_k if [106]:

$$P_k L_k F_k(x) > P_j L_j F_j(x) \qquad \text{for all } k \neq j \tag{3}$$

where $F_k(x)$ and $F_j(x)$ are the PDFs for classes C_k and C_j respectively, L_k is the loss function associated with misclassifying the vector as belonging to class C_j while it belongs to class C_k, L_j is the loss function associated with misclassifying the vector as belonging to class C_k while it belongs to class C_j, P_k and P_j are the prior probabilities of occurrence of the classes C_k and C_j, respectively. In many situations such as damage assessment problem, L and P are usually assumed to be equal for all classes. Hence, the key to using the decision rule given by Eq. (2) is to estimate the PDFs from the training patterns.PNN operates based on the concept of a nonparametric estimation technique known as Parzen windows classifier and its application to Bayesian statistics to estimate the PDFs for each classification class [58, 106, 114]. If the jth training pattern for class C_k is x_j, then the Parzen estimate of the PDF (F_k) for class C_k is [106]:

$$F_k(x) = \frac{1}{(2\pi)^{m/2}\eta^m}\frac{1}{n}\sum_{j=1}^{n} exp\left(-\frac{(x-x_j)^T(x-x_j)}{2\eta^2}\right) \tag{4}$$

or

$$F_k(x) = \frac{1}{(2\pi)^{m/2}\eta^m}\frac{1}{n}\sum_{j=1}^{n} exp - \left(\frac{\|x-x_j\|^2}{2\eta^2}\right) \tag{5}$$

where n is the number of training patterns of class C_k, m is the input space dimension, and η is an adjustable smoothing parameter. In fact, the parameters x_j and η represent the center and spread (or volume) of the Gaussian bell curve, respectively. The parameter η must be determined

experimentally [58, 106, 114]. Eq. (4) implies that any smooth density function can be expressed simply as the sum of small multivariate Gaussian distributions.

Fig. 15 shows a typical representation of the PNN architecture. As it is seen, the PNN architecture consists of four layers: (1) input layer, (2) pattern layer, (3) summation layer, and (4) a single-node output layer. The input layer includes the m input variables (x_1, x_2,…, x_m). All of the variables x are distributed by the input layer to all the neurons in the pattern layer. These layers are fully connected so that one neuron is allocated for each pattern in the training set. Thus, the number of nodes in the pattern layer is equal to the number of available training input vectors (n). The number of nodes in the summation layer is equal to the defined classes. A dot product operation is applied by each pattern neuron j to the input pattern vector x with a weight vector w_j such that $A_j = xw_j$. A transfer function in the form of $exp\left(\frac{A_j - 1}{\eta^2}\right)$ is applied to A_j *and* then it is outputted to the summation neuron [58, 106]. As both x and w_j are normalized to unit length, this is equivalent to performing the dot product operation:

$$exp\left(-\frac{(w_j - x)^T (w_j - x)}{2\eta^2}\right) \tag{6}$$

which can be written as:

$$exp\left(\frac{2x^T w_j - x^T x - w_j^T w_j}{2\eta^2}\right) \tag{7}$$

Since x and w_j are normalized to unit length, the dot products $x^T x$ and $w_j^T w_j$ are equal to 1. Thus, the above equation can be expressed as:

$$exp\left(\frac{x^T w_j - 1}{\eta^2}\right) \tag{8}$$

It can be observed that the transfer function $exp\left(\frac{z_j - 1}{\eta^2}\right)$ and the exponential term in Eq. (4) have the same form. It is necessary to compute this exponential term for each of the neurons in the pattern layer [58, 106].

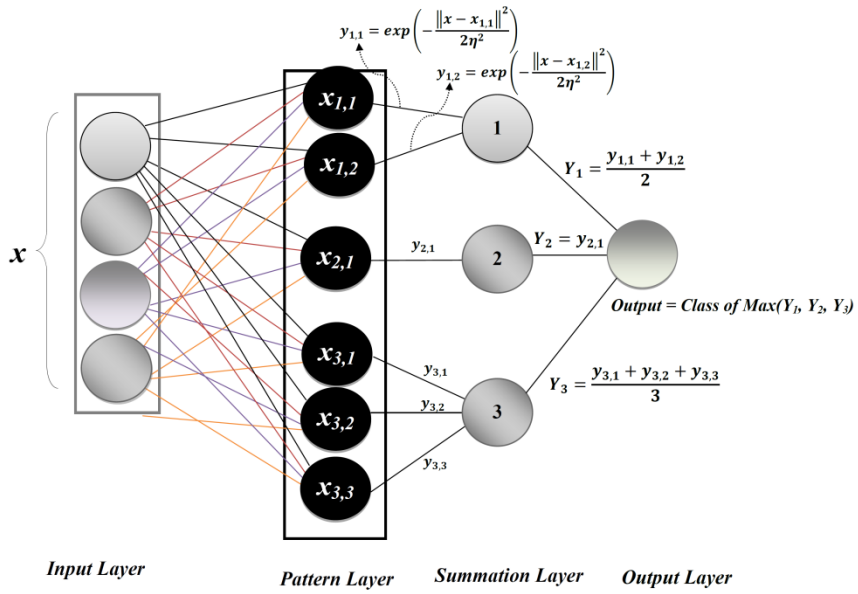

Fig. 15. A typical architecture of PNN with 4 input variables, 6 training instances, and 3 defined classes

The summation of units in the summation layer simply sums all the inputs from the pattern units that correspond to a given class. This results in the determination of the PDF of each category given by Eq. (4). In fact, there is one summation- layer neuron for each category. For instance, the output of the summation layer neuron corresponds to the class C_k is [106]:

$$C_k(x) = \sum_{j=1}^{n_k} exp\left(\frac{(x.w_{kj} - 1)}{\eta^2}\right) \quad (9)$$

Comparing Eq. (3) with Eq. (9), the constant term of Eq. (4) can be ignored. This results in the determination of the PDF of each category given by Eq. (4). It is worth mentioning that the transfer function is not limited to being an exponential or Gaussian. A number of different transfer functions are presented by Specht [107]. The smoothing parameter, η, has the same value throughout the network. Training of PNN can be regarded as finding the best η value for a set of vectors $\boldsymbol{x}$ which maximizes the classification accuracy of another independent set of vectors (testing data). The fourth layer of the network is the output-layer. This layer gives a binary output value corresponding to the highest PDF. The highest PDF indicates the best

classification or category choice for that pattern. In general, a PNN for M classes can be defined as follows:

$$Y_j(x) = \frac{1}{n_j}\sum_{i=1}^{n_j} exp\left(-\frac{\|x-x_{j,i}\|^2}{2\eta^2}\right), j = 1, \dots, M \quad (10)$$

where n_j denotes the number of data points in class j. PNN assigns x into class m if $Y_m(x) > Y_j(x)$, $j \in [1,\dots, M]$. $\|x\text{-}x_{j,i}\|^2$ is calculated as the sum of squares. e.g. if $x_{j,i} = [1,5]^T$, x = $[2,3]^T$, then $\|x\text{-}x_{j,i}\|^2 = (2 - 1)^2 + (3 - 5)^2 = 5$. The PNN classification procedure is illustrated in Fig. 16. As an example, the following three and two data points belong to Class 1 and Class 2, respectively.

Class 1: $x_{1,1} = (2, 1); x_{1,2} = (1, 2); x_{1,3} = (0, 2)$

Class 2: $x_{2,1} = (-2, 0); x_{2,2} = (-1, -2)$

The class label for the data sample $x = [1, 1.5]^T$ is required. Using the PNN Gaussian window function with $\eta = 1$, the PDFs for Class 1 and Class 2 at x are:

$$Y_1(x) = \frac{1}{3}\left[exp\left(-\frac{(1-2)^2 + (1.5-1)^2}{2(1)^2}\right) + exp\left(-\frac{(1-1)^2 + (1.5-1)^2}{2(1)^2}\right) + exp\left(-\frac{(1-0)^2 + (1.5-2)^2}{2(1)^2}\right)\right] = 0.651$$

$$Y_2(x) = \frac{1}{2}\left[exp\left(-\frac{(1-(-2))^2 + (1.5-0)^2}{2(1)^2}\right) + exp\left(-\frac{(1-(-1))^2 + (1.5-(-2))^2}{2(1)^2}\right)\right] = 0.002$$

Since $Y_1(x) > Y_2(x)$, $x = [1, 1.5]^T$ is classified as Class 1. The data points in the above example are shown in Fig. 16.

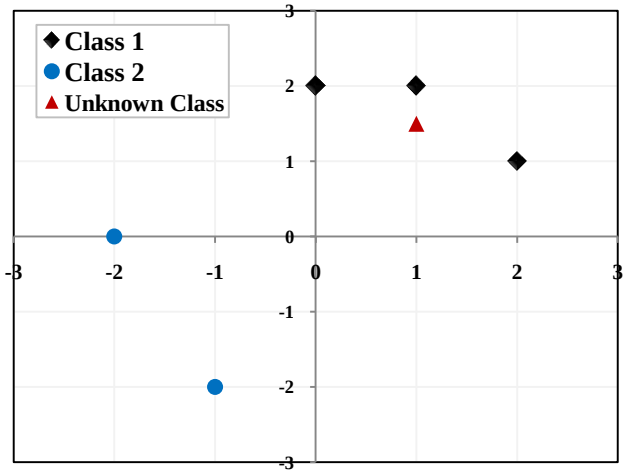

Fig. 16. Data points and their corresponding classes

4.2. Damage Detection for Simply Supported Beam

For the simply supported beam, several analyses are performed with 150, 100, 50, 25, 20, 15, 10 and 5 "randomly selected" elements (sensors). In order to have an insight into the effect of pre-determining of the location of the sensors, two separate scenarios are considered for sensor numbers equal to 10 and 5. For these cases, the sensors are assumed to be located in the mid-span of the beam and above the notch. As can be seen in Figs. 7 (a) to (c), this critical location is notably influenced by the applied load for both the intact and damaged cases. Each of the damage classes is represented by a dummy variable. The variables of 1 to 7 stand for intact beam, a/D = 0.05, a/D = 0.1, a/D = 0.2, a/D = 0.3, a/D = 0.4, and a/D = 0.45, respectively. For the first phase of the analyses, the damage state is considered to be a function of the following parameters:

$$Damagestate = f(X, Y, \mu, \sigma) \tag{11}$$

where,

X: Horizontal distance of the sensor from the beam center

Y: Vertical distance of the sensor from the beam center

μ: Mean of the strain distribution

σ: Standard deviation of the strain distribution

For the analysis, the generated data sets for each of the sensor configurations are randomly classified into three subsets: (1) calibration, (2) validation, and (3) test subsets. The calibration set is used to fit the models and the validation set is used to estimate the classification error for model selection [115]. For each of the sensor configurations, a number of repetitions with newly generated random locations are considered to guarantee that the models with the best performance on both the calibration and validation phases are derived. Finally, the testing set is employed for the evaluation of the generalization ability of the final chosen models. The calibration, validation and testing data are usually taken as 50-70%, 15-25% and 15-25% of all data, respectively [72, 115]. In the present study, 70% of the data vectors are used for the calibration process and about 15% of the data are taken as the validation data. The remaining of

the data sets are used for the testing of the obtained models. Table 3 shows the descriptive statistics of the μ and σ values for the entire elements.

Table 3. Descriptive statistics of the μ and σ values for the beam

Parameter	μ	σ
Mean	1.68E-05	6E-06
Median	1.68E-05	5.44E-06
Standard Deviation	7.22E-06	1.19E-05
Sample Variance	5.22E-11	1.42E-10
Kurtosis	466.3135	175.2442
Skewness	-20.4581	11.46525
Range	0.000186	0.000231
Minimum	-0.00017	9.73E-07
Maximum	1.97E-05	0.000232

Each calibration (training) sample is set as one neuron in the pattern layer of PNN. Thus, the number of neurons in the pattern layer of the PNN models made with 150, 100, 50, 25, 20, 15, 10 and 5 randomly selected elements is 731, 490, 245, 123, 74, 49, and 25, respectively. Neurons in the summation layer correspond to 7 damage patterns. An extensive trial study is performed to select the most relevant input parameters for the PNN model and the smoothing parameter (η). Several runs are conducted to obtain a parameterization of PNN with enough generalization. When presenting new input vectors, each neuron in the summation layer outputs the PDF estimations for each pattern at the test sample point. The pattern class with the largest PDF indicates the damage class of the current test sample. A Gaussian function is used as the window function for the PNN algorithm. The best classification results for different number of sensors are presented in Table 4. Based on the conducted runs, the models were not any sensitive to X and Y. That is to say, μ and σ can be considered as sufficient representatives of the damage progress. However, as can be observed in Table 4, the models provide good estimations of the damage on the calibration data but very poor performance on the validation and testing data.

Furthermore, slightly better results are provided by locating the 10 and 5 sensor numbers in the mid-span of the beam compared to the randomly distributed cases.

Table 4. The damage detection performance for the beam using X, Y, μ and σ as the predictor variables

Number of potential sensors	Damage Detection Performance (%)			Optimal smoothing parameter
	Calibration	Validation	Testing	
150	85%	24%	24%	1E-25
100	85%	30%	24%	1E-20
50	88%	21%	33%	1E-20
25	94%	19%	12%	1E-25
15	97%	25%	20%	1E-20
10	98%	0%	20%	1E-20
5	92%	20%	0%	1E-25
10 (Set)[1]	100%	9%	20%	1E-15
5 (Set)[2]	96%	20%	20%	1E-30

1 and 2: Sensors located in the mid-span of the beam, above the notch

Rationally, the closer the sensors to the notch are, the higher the damage detection accuracy is. For the cases where the potential sensors are at a great distance from the imposed damage, the sensor would not have a sense of damage. Thus, as discussed before, a new strategy is defined to improve the damage detection performance. On its basis, it is decided to use both the information provided by one sensor and also the general information supplied by the other sensors in that specific sensor configuration (group of sensors). In this case, even if one sensor does not sense

the damage, the group effect will help detect the damage. To tackle this issue, a set of new input parameters are introduced to the formulation of the damage state as follows:

$$Damagestate = f\left(X, Y, \mu, \sigma, \mu_D, \sigma_D, \mu_S, \sigma_S, Z_{\mu 1}, Z_{\sigma 1}, Z_{\mu 2}, Z_{\sigma 2}\right) \quad (12)$$

where,

$\mu_D: \frac{\mu}{\mu_{ave}}$ and μ_{ave} is the average of μ of all sensors for a specific damage scenario that μ belongs.

$\sigma_D: \frac{\sigma}{\sigma_{ave}}$ and σ_{ave} is the average of σ of all sensorsfor a specific damage scenario that σ belongs.

$\mu_S: \mu - \mu_{ave}$ and μ_{ave} is the average of μ of all sensorsfor a specific damage scenario

$\sigma_S: \sigma - \sigma_{ave}$ and σ_{ave} is the average of σ of all sensorsfor a specific damage scenario

$Z_{\mu 1}: \frac{\mu - \mu_{ave}}{\mu_{STD}}$ and μ_{STD} is the standard deviation of μ of all sensors for a specific damage scenario

$Z_{\sigma 1}: \frac{\sigma - \sigma_{ave}}{\sigma_{STD}}$ and σ_{STD} is the standard deviation of σ of all sensorsfor a specific damage scenario

$$Z_{\mu 2}: \frac{\mu - \mu_{ave}}{\sigma_{ave}}$$

$$Z_{\sigma 2}: \frac{\sigma - \mu_{ave}}{\sigma_{ave}}$$

In fact, $Z_{\mu 1}$ and $Z_{\sigma 1}$ are z-score functions. $Z_{\mu 2}$ and $Z_{\sigma 2}$ are functions defined in this study inspired by the form of the conventional z-score function. As can be observed, the considered input variables efficiently take into account the sensor group effect which would improve the detection performance, specifically for low number of sensors. For example, assume the case where 10 sensors with random locations are used for the damage detection and one is located at the corner of the beam. For sure, μ and σ of the sensor at the corner will not have sufficient information for detecting the damage state. This is while by using parameters such as $\mu_D, \sigma_D, \mu_S, \sigma_S, Z_{\mu 1}, Z_{\sigma 1}, Z_{\mu 2}$, and $Z_{\sigma 2}$, the information from the sensors distributed along the beam would enhance the classification accuracy. Similar to the previous stage, several runs are conducted to obtain a parameterization of PNN with enough generalization.

After extensive preliminary runs, it is found that the parameters defined in Eq. (12) do not provide good estimations when used together. A possible reason is that each set of the input parameters require a specific smoothing parameter. Also, it is revealed that X, Y, μ, and σ even decrease the detection performance when used with other parameters. However, the input parameters for the final analyses are categorized into two different groups: (1) $\mu_D, \sigma_D, \mu_S, \sigma_S$, and (2) $Z_{\mu 1}, Z_{\sigma 1}, Z_{\mu 2}, Z_{\sigma 2}$. Tables 5 and 6 present the best classification results for different number of sensors for two different input categories. For a better visualization of the results, the performance of the models on the validation and testing data is separately shown in Fig. 17. As can be observed from Tables 4 to 6 and Fig. 17, introducing the new set of the input parameters (i.e., $\mu_D, \sigma_D, \mu_S, \sigma_S, Z_{\mu 1}, Z_{\sigma 1}, Z_{\mu 2}$, and $Z_{\sigma 2}$) to the modeling process results in a significant improvement of the damage detection performance. The models using $\mu_D, \sigma_D, \mu_S, \sigma_S, Z_{\mu 1}, Z_{\sigma 1}, Z_{\mu 2}$, and $Z_{\sigma 2}$ as the predictor variables have a very good performance both on the calibration data and on the validation and testing data. Expectedly, the precision of the models decreases with decreasing the number of sensors. Moreover, it can be seen that, nearly in all cases, the models built with $Z_{\mu 1}, Z_{\sigma 1}, Z_{\mu 2}$, and$Z_{\sigma 2}$ have a better performance than those made usingμ_D, σ_D, μ_Sandσ_S as the input parameters. Also, the models developed with the second set of the predictor variables for the cases of 10 and 5 sensor numbers in the mid-span of the beam provide a significantly better performance than those established using only X, Y, μ and σ. Considering the above explanations, it can be concluded that $\mu_D, \sigma_D, \mu_S, \sigma_S, Z_{\mu 1}, Z_{\sigma 1}, Z_{\mu 2}$, and $Z_{\sigma 2}$ contain sufficient information for the detection of the damage state. Besides, Fig. 18 presents the detailed classification performance of the derived models on testing data with confusion matrixes. A confusion matrix [116] contains information about actual and predicted classifications. Each column of the matrix represents the instances in a predicted class, while each row represents the instances in an actual class.

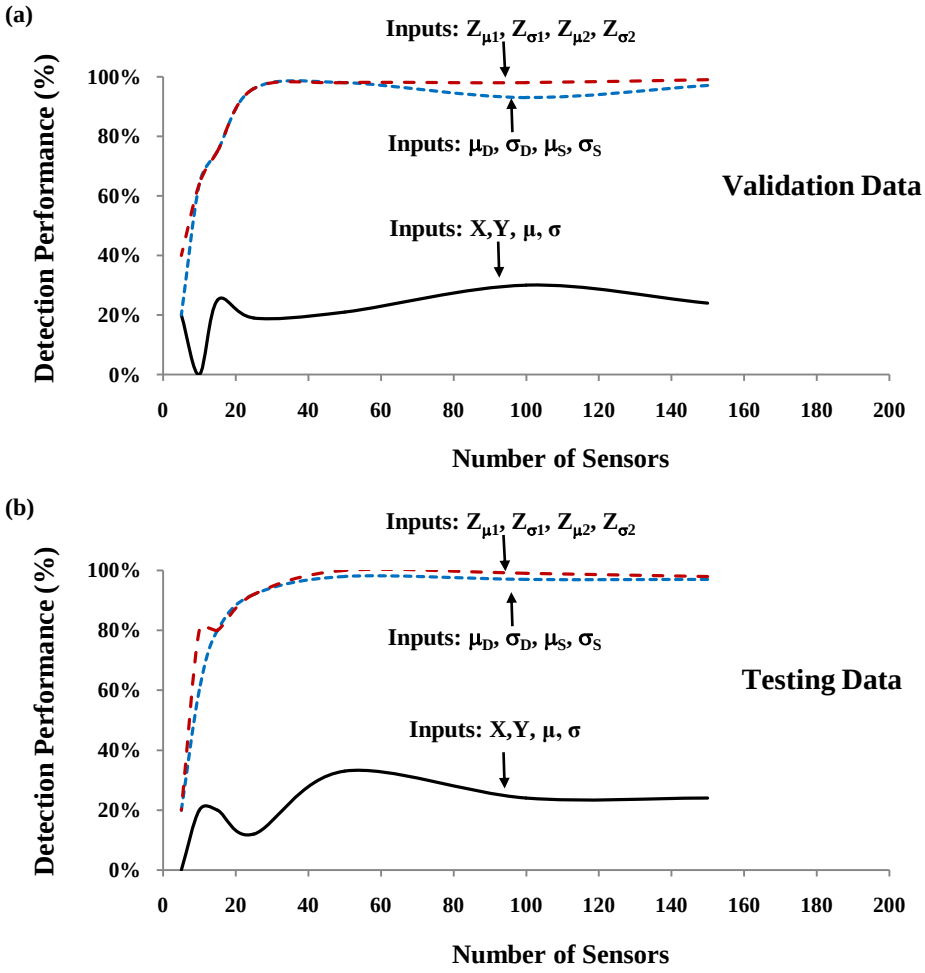

Fig. 17. A visual comparison of the performance of the models developed using different sets of input parameters on the validation and testing data

Table 5. The damage detection performance for the beam using $\mu_D, \sigma_D, \mu_S, \sigma_S$ as the predictor variables

Number of potential sensors	Damage Detection Performance (%)			Optimal smoothing parameter
	Calibration	Validation	Testing	
150	99%	97%	97%	25E-4
100	100%	93%	97%	1E-4
50	100%	98%	98%	1E-4
25	100%	96%	92%	1E-4
15	96%	75%	80%	1E-4
10	92%	64%	60%	1E-5
5	96%	20%	20%	1E-4
10 (Set)	96%	73%	60%	1E-4
5 (Set)	100%	80%	80%	1E-4

Table 6. The damage detection performance for the beam using $Z_{\mu 1}, Z_{\sigma 1}, Z_{\mu 2}$, and $Z_{\sigma 2}$ as the predictor variables

Number of potential sensors	Damage Detection Performance (%)			Optimal smoothing parameter
	Calibration	Validation	Testing	
150	100%	99%	98%	1E-1
100	100%	98%	99%	1E-1
50	100%	98%	100%	1E-1
25	100%	96%	92%	1E-2
15	97%	75%	80%	1E-4
10	82%	64%	80%	1E-1
5	92%	40%	20%	1E-1
10 (Set)	96%	91%	90%	1E-3
5 (Set)	100%	80%	80%	1E-1

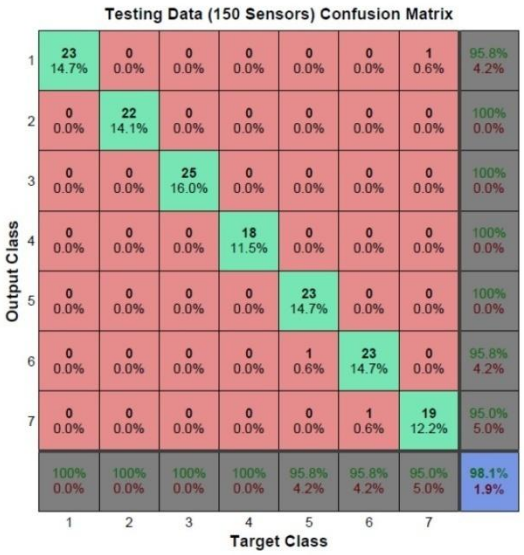
Testing Data (150 Sensors) Confusion Matrix
Output Class
Target Class
23 14.7%
22 14.1%
25 16.0%
18 11.5%
23 14.7%
23 14.7%
19 12.2%
1 0.6%
95.8% 4.2%
98.1% 1.9%

(a)

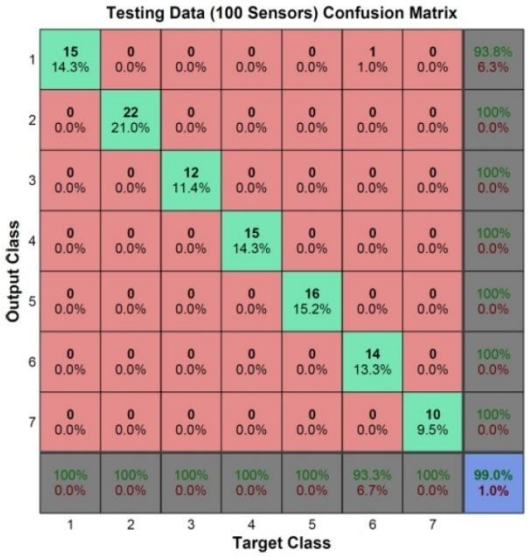
Testing Data (100 Sensors) Confusion Matrix
Output Class
Target Class
15 14.3%
22 21.0%
12 11.4%
15 14.3%
16 15.2%
14 13.3%
10 9.5%
1 1.0%
93.8% 6.3%
99.0% 1.0%

(b)

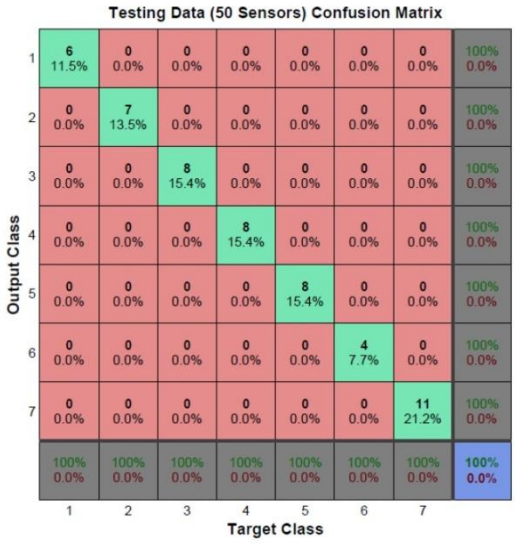
Testing Data (50 Sensors) Confusion Matrix
Output Class
Target Class
6 11.5%
7 13.5%
8 15.4%
8 15.4%
8 15.4%
4 7.7%
11 21.2%
100% 0.0%

(c)

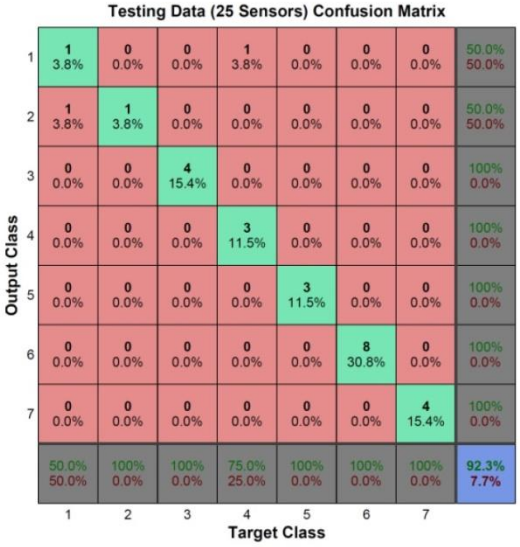
Testing Data (25 Sensors) Confusion Matrix
Output Class
Target Class
1 3.8%
1 3.8%
1 3.8%
4 15.4%
3 11.5%
3 11.5%
8 30.8%
4 15.4%
50.0% 50.0%
92.3% 7.7%

(d)

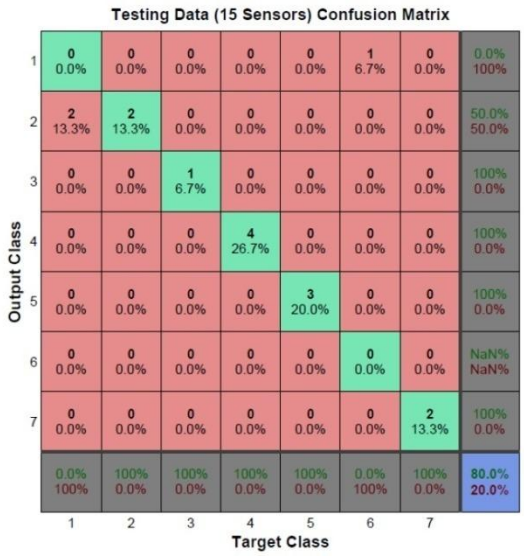
Testing Data (15 Sensors) Confusion Matrix
Output Class
Target Class
1 6.7%
2 13.3%
2 13.3%
1 6.7%
4 26.7%
3 20.0%
2 13.3%
0.0% 100%
80.0% 20.0%

(e)

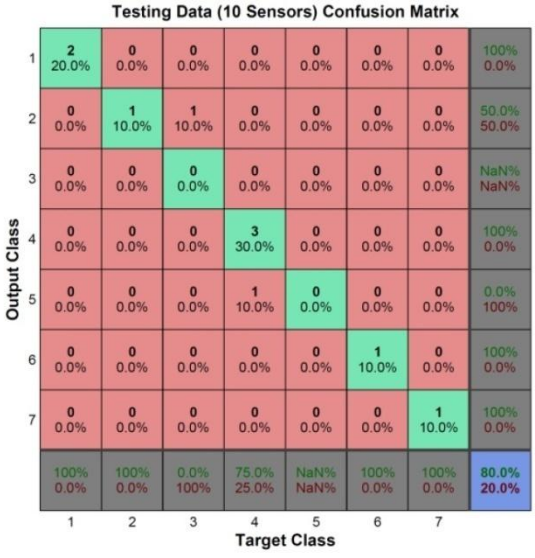
Testing Data (10 Sensors) Confusion Matrix
Output Class
Target Class
2 20.0%
1 10.0%
1 10.0%
3 30.0%
1 10.0%
1 10.0%
1 10.0%
80.0% 20.0%

(f)

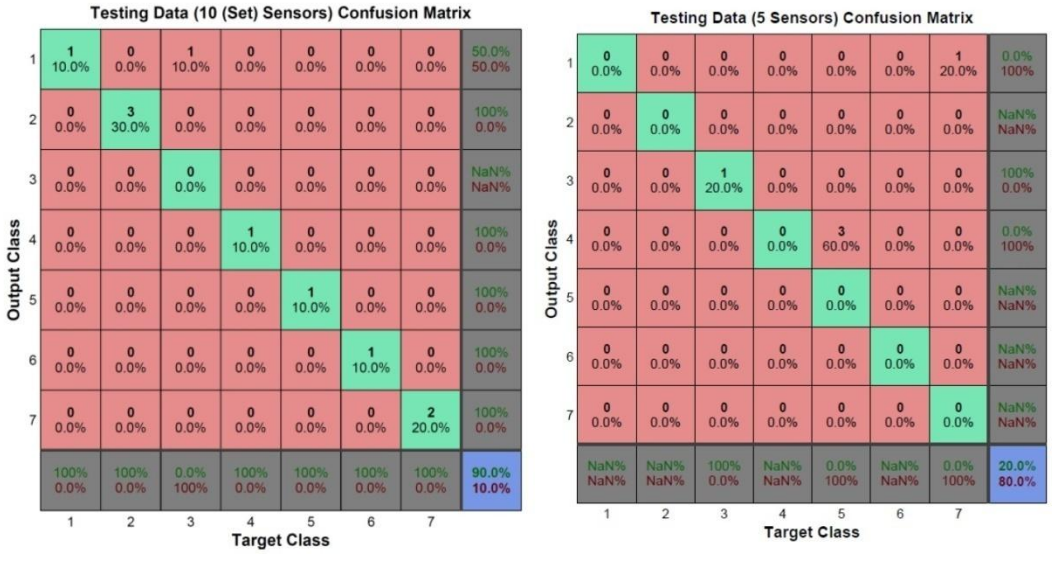

(g) **(h)**

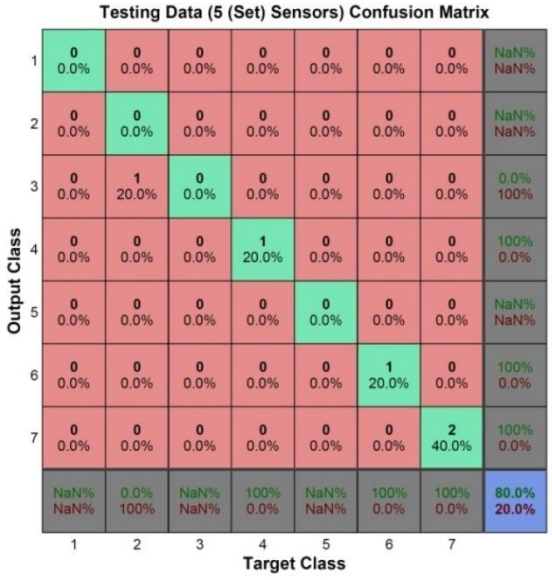

(i)

Fig. 18. Confusion matrixes of the beam models for different number of sensors

4.2.1. Uncertainty Analysis

As it is known, the model error exists even for a well calibrated FEM model. This error may be caused by the boundary condition, distribution of the structural stiffness, uncertainty of material, etc. Moreover, the real structure might be subjected to environmental effects and operational states such as varying temperature and measurement noise [106]. PNN has noticeable merits in noisy conditions as it describes measurement data in a Bayesian probabilistic approach [117]. Despite this capability, adding noise to the data in order to simulate the error of the analytical

model and the effect of noise on the actual measurement vectors enhances the reliability of the proposed method. Thus, in this study, the calibration, validation and testing sets are polluted with random noise to simulate the performance of real sensors. To this aim, Gaussian noise with a mean value of zero and standard deviation equal to one standard deviation of the measured data is added to the input vectors. The noise pollution verification phase has been done only for the best models that are developed using $Z_{\mu 1}, Z_{\sigma 1}, Z_{\mu 2}$, and$Z_{\sigma 2}$ (see Table 3). Different noise levels are taken for the analysis (5%, 10%, 20%, 30%, and 50%). The PNN algorithm is run for all the combinations shown in Table 6 with noise-polluted data. Table 7 and Fig. 19 visualize the best classification results for different number of sensors with various noise levels. Comparing the results shown in Tables 3 and 6, 7 and Fig. 19, it can be observed that increasing the noise level does not influence on the performance of the models on the calibration data. For the validation and testing data, the trends of the results are complicated. In these cases, it can be seen that the identification accuracies of the models gradually decrease with the increase of the noise level. The results for the testing data indicate that nearly all of the models have a good accuracy for noise levels up to 20%. On the other hand, the performance of the models subjected to higher noise levels, in particular 30 and 50%, does not remain satisfactory. This is more evident for the 5 and 10 sensor numbers.

Table 7. The damage detection performance of the best models for beam for various noise levels

Number of potential sensors	Noise Level	Damage Detection Performance (%)			Optimal smoothing parameter
		Calibration	Validation	Testing	
150	5%	100%	97%	97%	1E-2
	10%	100%	96%	94%	1E-2
	20%	100%	94%	90%	1E-2
	30%	100%	85%	83%	1E-2
	50%	100%	78%	78%	1E-2
100	5%	100%	94%	97%	1E-2
	10%	100%	92%	92%	1E-2
	20%	100%	90%	90%	1E-2
	30%	100%	82%	86%	1E-2
	50%	100%	72%	72%	1E-2
50	5%	100%	87%	94%	1E-2
	10%	100%	81%	90%	1E-2
	20%	100%	89%	79%	1E-2
	30%	100%	68%	65%	1E-2
	50%	100%	58%	62%	1E-2
25	5%	100%	92%	92%	1E-2
	10%	100%	69%	92%	1E-2
	20%	100%	65%	69%	1E-2
	30%	100%	65%	62%	1E-2
	50%	100%	35%	65%	1E-2
15	5%	100%	75%	73%	1E-2
	10%	100%	69%	73%	1E-2
	20%	100%	69%	67%	1E-2
	30%	100%	69%	60%	1E-2
	50%	100%	38%	40%	1E-2
10	5%	96%	64%	70%	1E-1
	10%	94%	55%	70%	1E-1
	20%	98%	55%	70%	1E-1
	30%	98%	45%	40%	1E-1
	50%	100%	45%	30%	1E-1

	5%	92%	60%	20%	1E-1
	10%	100%	80%	20%	1E-1
5	20%	100%	60%	0%	1E-1
	30%	100%	20%	0%	1E-3
	50%	100%	20%	0%	1E-3
	5%	100%	73%	70%	1E-2
	10%	100%	55%	70%	1E-2
10 (Set)	20%	100%	64%	50%	1E-1
	30%	98%	64%	30%	1E-1
	50%	98%	36%	30%	1E-1
	5%	100%	40%	80%	1E-1
	10%	100%	40%	80%	1E-1
5 (Set)	20%	100%	20%	60%	1E-1
	30%	100%	40%	20%	1E-1
	50%	100%	20%	20%	1E-1

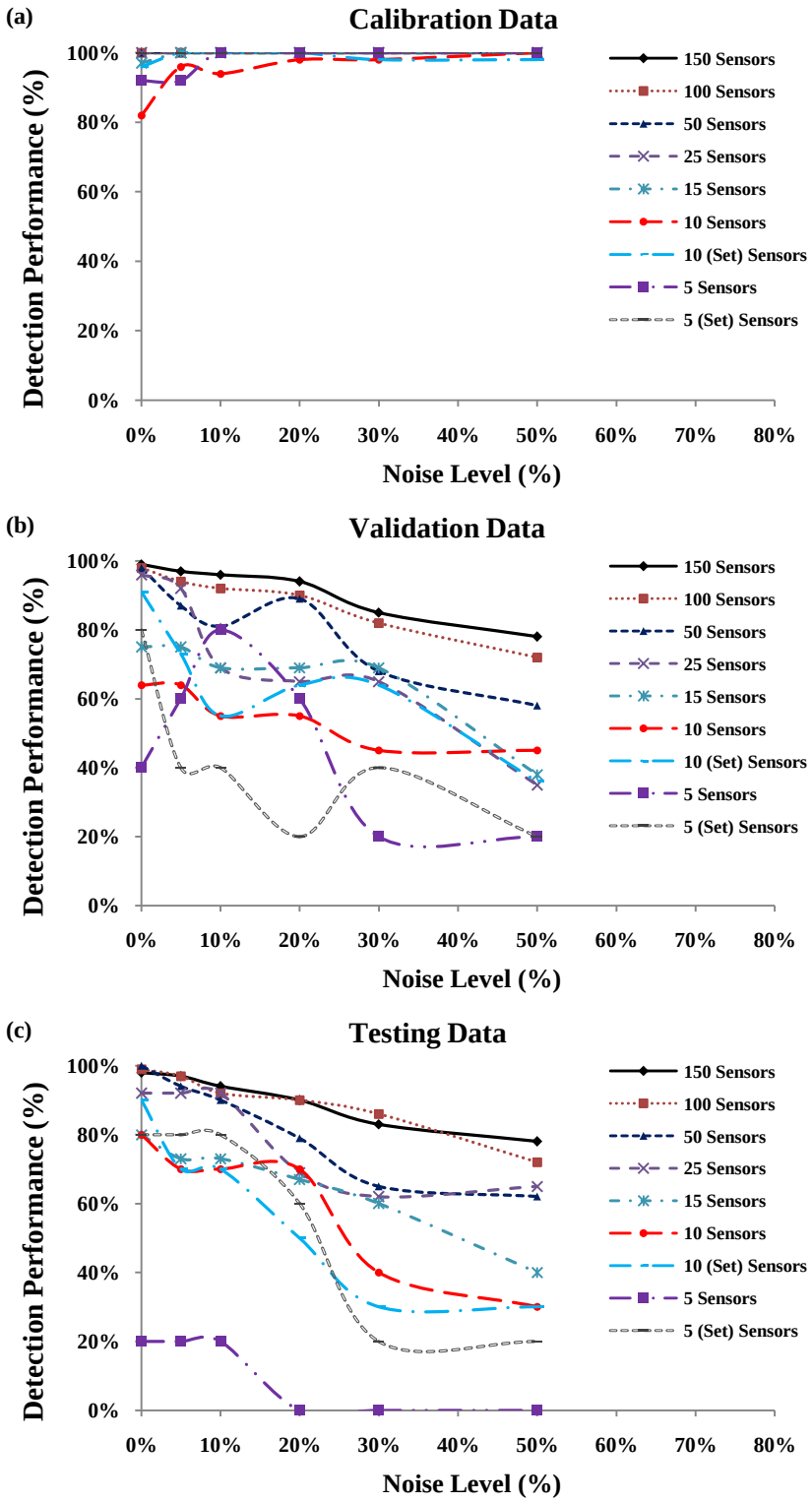

Fig. 19. The damage detection accuracy of the best models versus the noise levels for different number of sensors

4.3. Damage Detection for the Gusset Plate

The observations from the first stage of method verification provide valuable information to tackle the geometrically complicated case of gusset plate. For this case, in addition to the randomize configuration of the sensors, organized positioning of the sensors are also considered. As described in Section 3.2, the information for 448 data acquisition points is extracted for the analysis. However, considering high number of sensors is neither reasonable nor economic in practical applications. Thus, for the second stage of the performance verification, a maximum of 224 sensors is taken into account. The analyses are performed with 224, 112, 56, and 28 organized and randomly selected sensors. Similar to Case I, different pre-determined configuration schemes with 24, 28, 30, 42, 53, 57, and 64 sensors are also considered to assess the importance of locating the sensors at probable critical regions. Fig. 20 shows a schematic representation of the sensor configurations. In this figure, black and red cells represent the sensors. The red cells show the sensors that do not sense damage in all of the damage states. Since such sensors do not record any information, they are excluded from the analyses. The black cells define the active sensors. Based on the results obtained in the first stage (Table 3 and Fig. 17), it is revealed that X, Y, μ, and σ cannot be solely used for damage detection. Moreover, among different defined input features, $Z_{\mu 1}, Z_{\sigma 1}, Z_{\mu 2},$ and $Z_{\sigma 2}$ are the most efficient damage indicator variables. Consequently, these four input features are used for detecting the damage states introduced to the gusset plate. The available data for each of the sensor configurations are randomly divided into three calibration (70% of the data), validation (15% of the data), and testing (15% of the data) subsets. The descriptive statistics of the μ and σ values for the entire elements is shown in Table 8. As discussed before, for each of the randomized sensor configurations, a number of repetitions are considered to guarantee that the models with the best performance on both the calibration and validation phases are developed. Evidently, this issue is of great importance for low number of sensors.

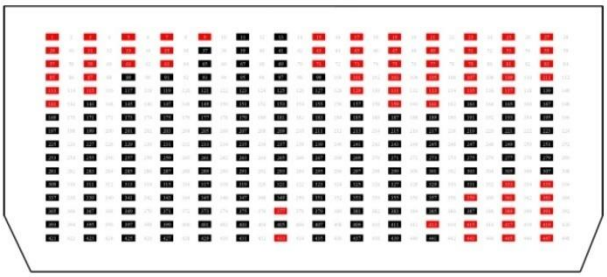

(a) 224 Organized Sensors (156 Active)

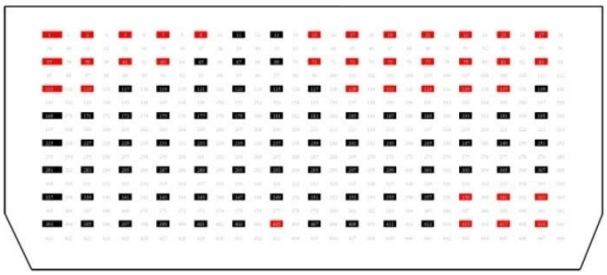

(b) 112 Organized Sensors (75 Active)

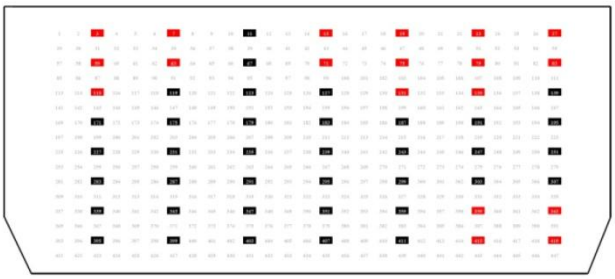

(c) 56 Organized Sensors (37 Active)

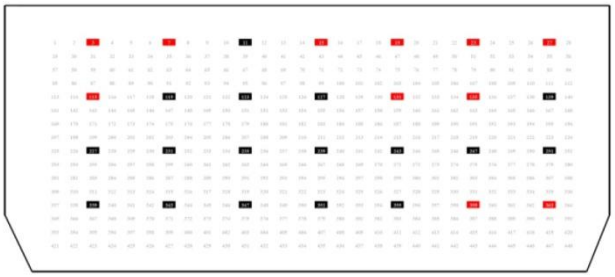

(d) 28 Organized Sensors (17 Active)

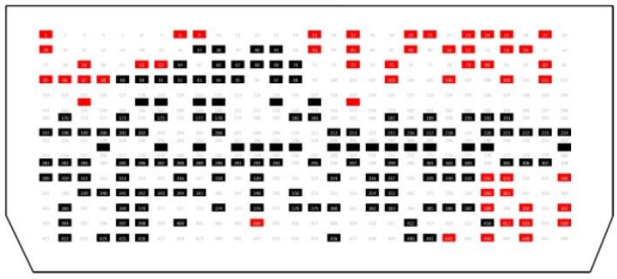

(e) 224 Randomized Sensors (168 Active)

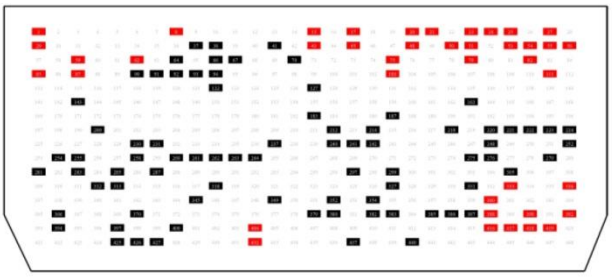

(f) 112 Sensors (72 Active)

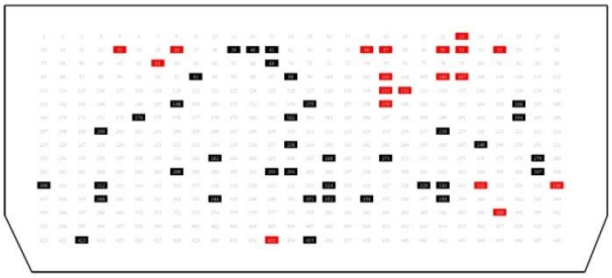

(g) 56 Randomized Sensors (37 Active)

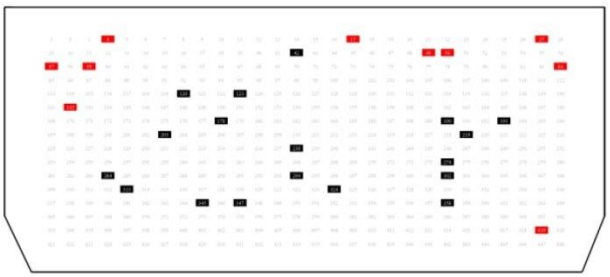

(h) 28 Sensors (17 Active)

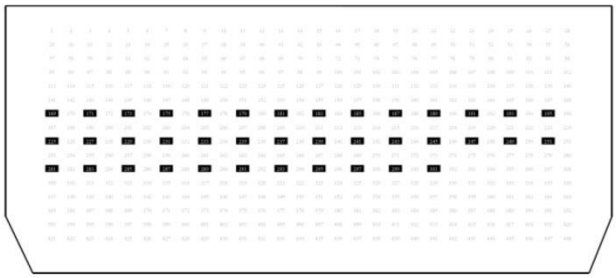

(i) 24 Sensors at Specified Locations

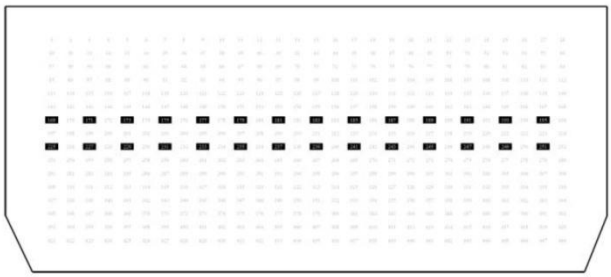

(j) 28 Sensors at Specified Locations

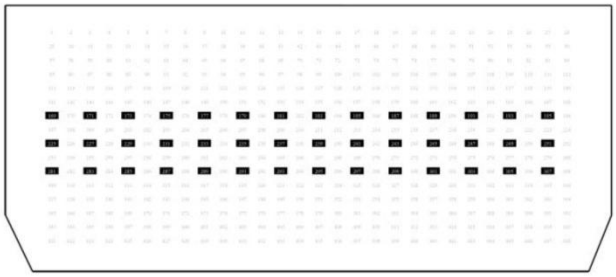

(k) 42 Sensors at Specified Locations

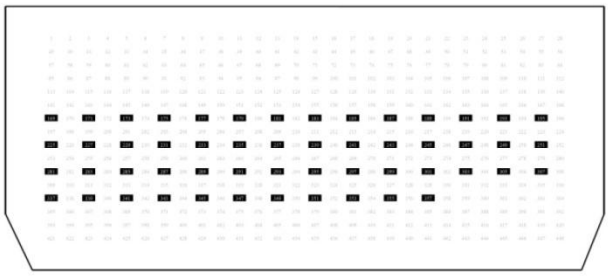

(l) 53 Sensors at Specified Locations

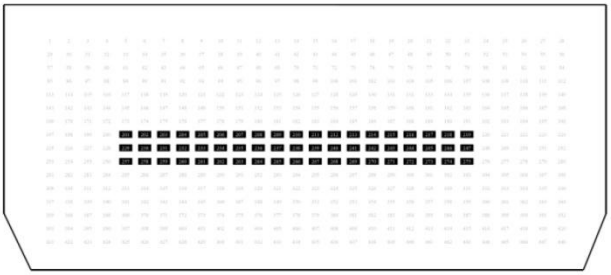

(m) 57 Sensors at Specified Locations

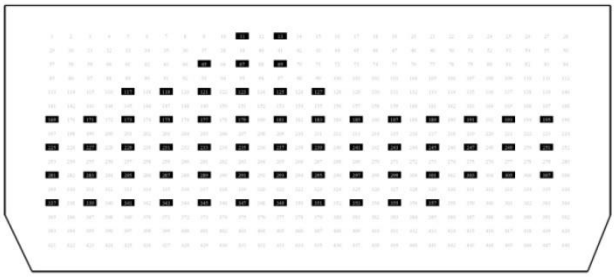

(n) 64 Sensors at Specified Locations

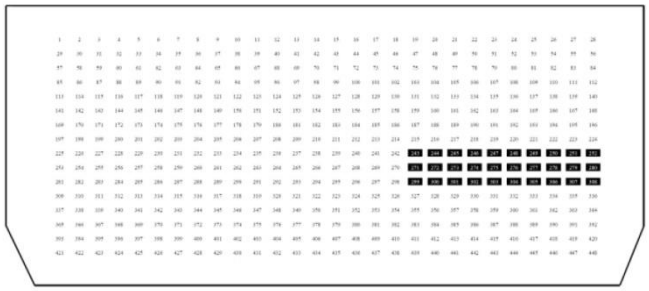

(o) 30 Sensors at Critical Location under the Notch

Fig. 20. A schematic representation of the sensor configurations for the gusset plate

Table 8. Descriptive statistics of the μ and σ values for the gusset plate

Parameter	μ	σ
Mean	1.68E-05	6.00E-06
Median	1.68E-05	5.44E-06
Standard Deviation	7.22E-06	1.19E-05
Sample Variance	5.22E-11	1.42E-10
Kurtosis	4.66E+02	1.75E+02
Skewness	-2.05E+01	1.15E+01
Range	1.86E-04	2.31E-04
Minimum	-1.70E-04	9.73E-07
Maximum	1.97E-05	2.32E-04

The number of neurons in the pattern layer of the PNN models made with 156, 75, 37, and 17 organized (active) sensors is 1638, 788, 389, and 179, respectively. These numbers for the final models with 168, 72, 37, and 17 randomly selected (active) sensors are 1764, 830, 389, and 179, respectively. Moreover, for the pre-determined configuration schemes with 64, 57, 53, 42, 30, 28, and 24 sensors, the number of neurons in the PNN's pattern layer is 672, 588, 557, 441, 315, 294, and 252, respectively. Neurons in the summation layer correspond to 15 damage patterns. Selection of the η values to find the optimal PNN models is based on extensive trial and error study. Furthermore, the algorithm is run several times to obtain a parameterization of PNN with enough generalization. A Gaussian function is adopted as the window function for the PNN algorithm. The best classification results for different number of sensors are presented in Table 9. In order to have an insight into the area covered by the sensors, the ratio of the area of sensors in each configuration to the area of the plate (Area Ratio) is also shown in Table 9. In order to visualize the detailed classification performance of the derived models on testing data, the corresponding confusion matrixes are given in Fig. 21.

As it is seen, the model with 156, 75, 37, and 17 organized sensors have a very good performance on the calibration, validation and testing data. The performance of the models build for 168 and 72 randomly selected sensors is also very satisfying. As expected, the precision of the models decreases with decreasing the number of sensors. However, considering the Area Ratio values, it is seen that even for 168 randomized sensors, only 0.39% of the plate is covered by the sensors (less than 1%). This is indeed a very low rate for achieving such high detection accuracy. On the other hand, for the pre-determined configuration schemes, only 64 and 30 sensors provide acceptable results. This indicates that organized and randomized distribution of the sensors can be a more effective strategy for increasing the detection precision. It is worth mentioning that by decreasing the number of damage classes, the accuracy of the models remarkably increases. For instance, the detection accuracy of the 17 organized sensors for 8 damage classes is equal to 100%, 85% and 90% on the calibration, validation and testing data,

respectively. For the 37 active organized sensors, these values are, respectively, equal to 100%, 91% and 86% on the calibration, validation and testing data. Thus, it is possible to reduce the number of sensors and yet have good detection accuracy by decreasing the number of damage classes.

Table 9. The damage detection performance for the gusset plate using $Z_{\mu 1}, Z_{\sigma 1}, Z_{\mu 2}$, and$Z_{\sigma 2}$ as the predictor variables

		Damage Detection Performance (%)				
	Number of potential sensors	Calibration	Validation	Testing	Area Ratio	Optimal smoothing parameter
Organized Location	224 (156*)	100%	87%	87%	0.390%	1E-5
	112 (75)	100%	86%	90%	0.195%	1E-5
	56 (37)	99%	66%	72%	0.097%	1E-4
	28 (17)	100%	68%	76%	0.049%	1E-5
Randomized Location	224 (168)	99%	94%	94%	0.390%	1E-5
	112 (72)	98%	86%	84%	0.195%	1E-5
	56 (37)	99%	46%	53%	0.097%	1E-4
	28 (18)	100%	30%	33%	0.049%	1E-4
Specified Location	24	100%	30%	33%	0.042%	1E-3
	28	100%	37%	29%	0.049%	1E-3
	42	100%	27%	38%	0.073%	1E-4
	53	99%	51%	52%	0.092%	1E-2
	57	99%	51%	52%	0.099%	1E-2
	64	100%	74%	74%	0.111%	1E-2
	30**	98%	59%	66%	0.052%	5E-7

* The numbers in the parentheses represent the active sensors for each configuration.

**The sensors are located under the notch.

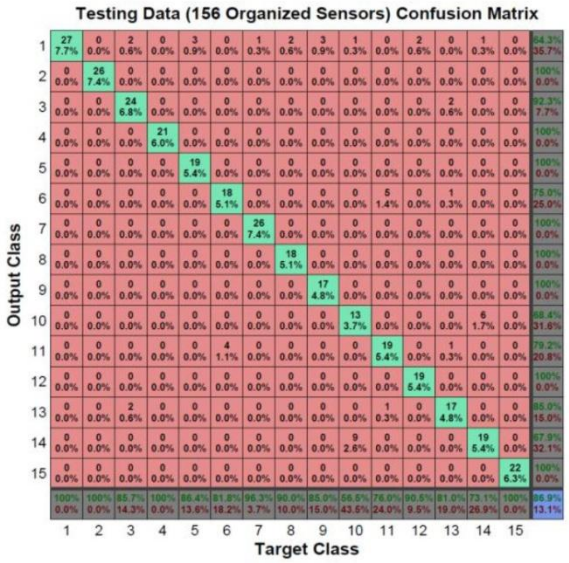
Testing Data (156 Organized Sensors) Confusion Matrix
Output Class
Target Class

(a)

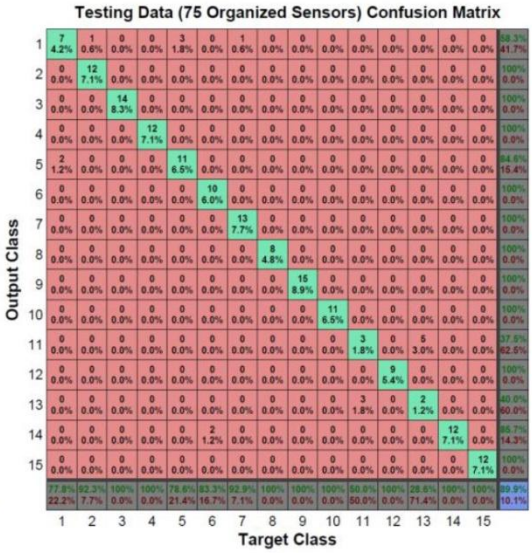
Testing Data (75 Organized Sensors) Confusion Matrix
Output Class
Target Class

(b)

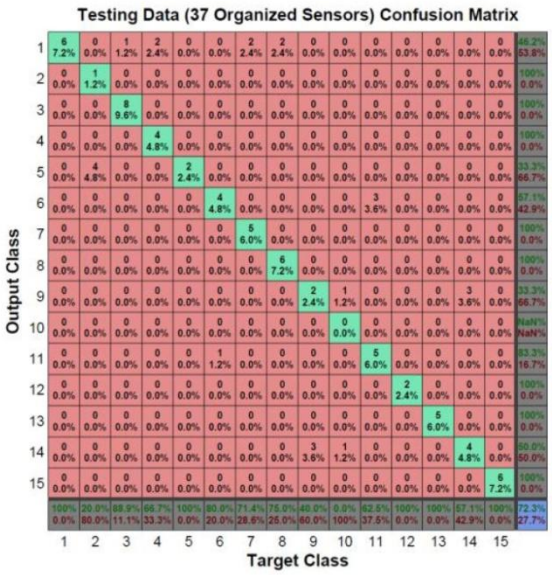
Testing Data (37 Organized Sensors) Confusion Matrix
Output Class
Target Class

(c)

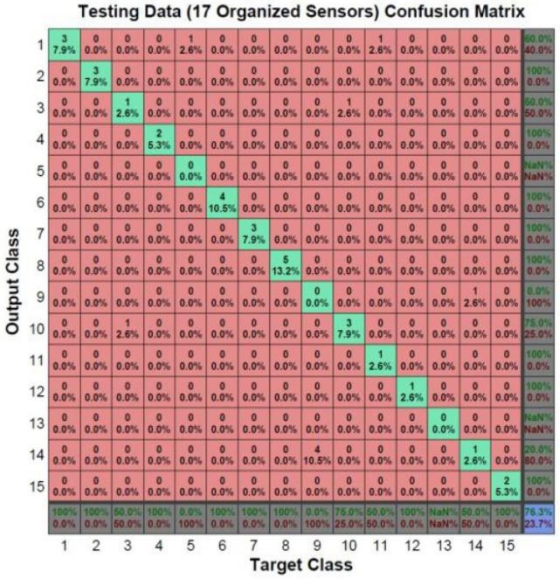
Testing Data (17 Organized Sensors) Confusion Matrix
Output Class
Target Class

(d)

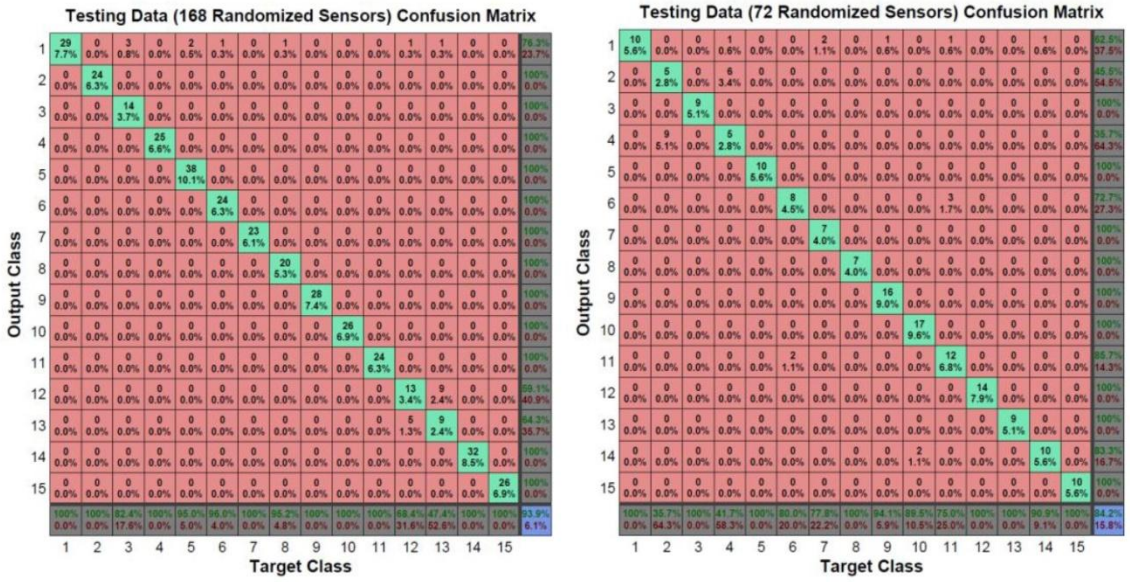

(e) (f)

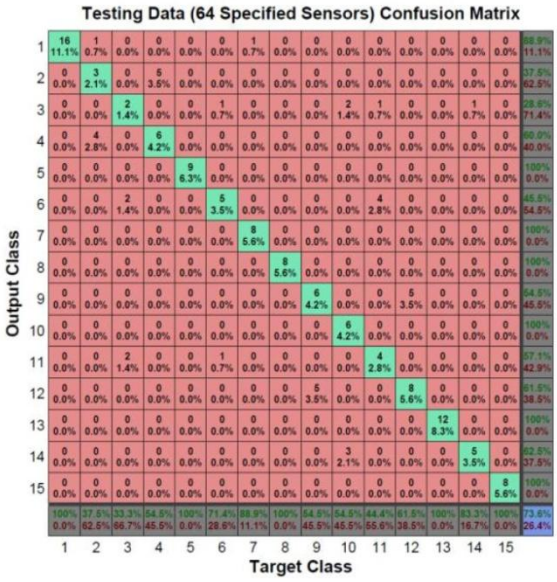

(g)

Fig. 21. Confusion matrixes of the best gusset plate models for different number of sensors

4.3.1. Uncertainty Analysis

In order to analyze the uncertainties in predictions, the calibration, validation and testing sets are polluted with random noise. Similar to the case of simply supported beam, Gaussian noise with a mean value of zero and standard deviation equal to one standard deviation of the measured data is added to the input vectors. The noise pollution verification phase has been done only for the best models shown in Table 9. That is, the models for 156, 75, 37, and 17 organized sensors, 168

and 72 randomly selected sensors, and 64 sensors at specified locations are chosen for the uncertainty analysis. Referring to the uncertainty analyses of the beam shown in Table 4, the performance of the models subjected to 30% and 50%noise levels is not satisfactory. Therefore, for the gusset plate case, only 5%, 10%, 20%, and 30%noise levels are considered. The PNN algorithm is run for all the chosen combinations. Table 10 and Fig. 22 present the best classification results for different number of sensors with various noise levels.

Comparing the results shown in Tables 9 and 10 and Fig. 22, it is seen that increasing the noise level even up to 30% does not influence the performance of the models build for 168 and 72 randomly selected sensors. Also, the performance of the models for 156 and 75 organized sensors is acceptable up to about 20% noise level. In all cases, it can be seen that the identification accuracies of the models gradually decrease with the increase of the noise level. Besides, the model for 64 sensors at specified locations has an acceptable accuracy only for 10% noise level.

Table 10. The damage detection performance of the best gusset plate models for various noise levels

	Number of potential sensors	Noise Level	Damage Detection Performance (%)			Optimal smoothing parameter
			Calibration	Validation	Testing	
Organized Location	156	5%	85%	70%	70%	5E-3
		10%	80%	68%	69%	5E-3
		20%	82%	68%	69%	5E-3
		30%	83%	64%	65%	5E-3
	75	5%	84%	73%	74%	1E-2
		10%	88%	73%	72%	1E-2
		20%	89%	72%	70%	1E-2
		30%	89%	65%	69%	1E-2
	37	5%	71%	54%	55%	1E-2
		10%	79%	48%	54%	1E-2
		20%	86%	52%	53%	1E-2
		30%	90%	46%	53%	1E-2
	17	5%	87%	53%	58%	1E-2
		10%	94%	53%	53%	1E-2
		20%	95%	53%	58%	1E-2

		30%	98%	53%	45%	1E-2
Randomized Location	168	5%	94%	91%	91%	1E-2
		10%	95%	92%	92%	1E-2
		20%	95%	90%	88%	1E-2
		30%	96%	86%	88%	1E-2
	72	5%	95%	72%	70%	1E-3
		10%	97%	75%	68%	1E-3
		20%	91%	75%	69%	1E-2
		30%	91%	71%	69%	1E-3
Specified Location	64	5%	95%	52%	59%	1E-3
		10%	100%	49%	53%	1E-3
		20%	99%	47%	43%	1E-3
		30%	100%	35%	44%	1E-3

(a)

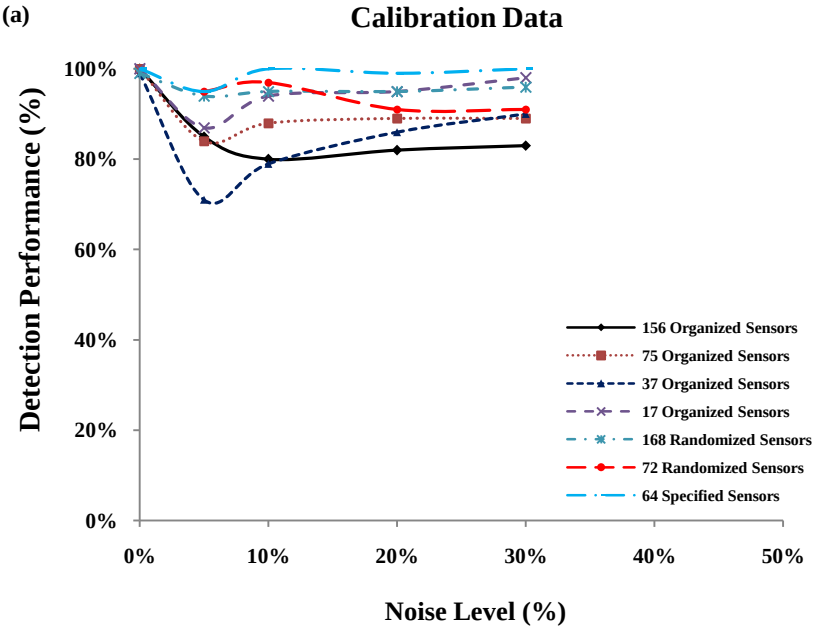
Calibration Data
Detection Performance (%)
100%
80%
60%
40%
20%
0%
0%
10%
20%
30%
40%
50%
Noise Level (%)
156 Organized Sensors
75 Organized Sensors
37 Organized Sensors
17 Organized Sensors
168 Randomized Sensors
72 Randomized Sensors
64 Specified Sensors

(b)

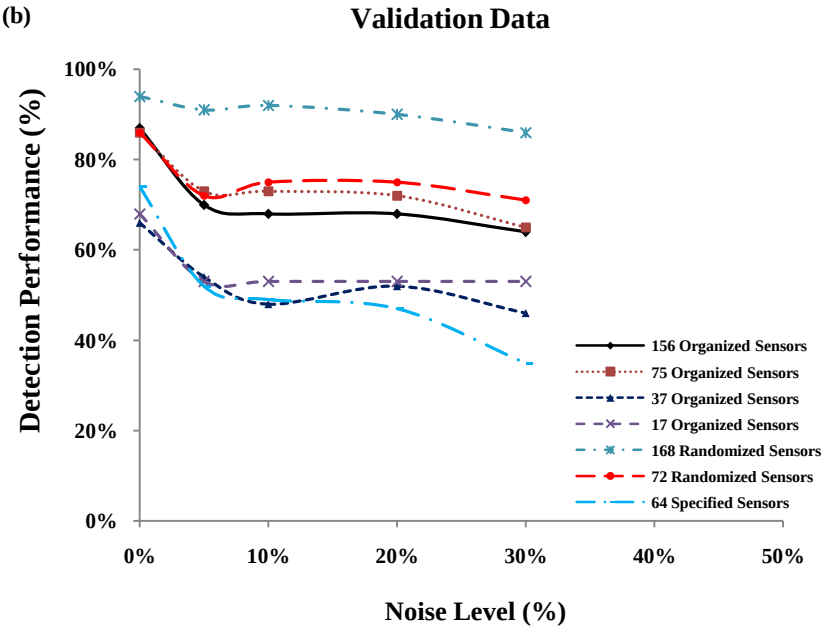
Validation Data
Detection Performance (%)
100%
80%
60%
40%
20%
0%
0%
10%
20%
30%
40%
50%
Noise Level (%)
156 Organized Sensors
75 Organized Sensors
37 Organized Sensors
17 Organized Sensors
168 Randomized Sensors
72 Randomized Sensors
64 Specified Sensors

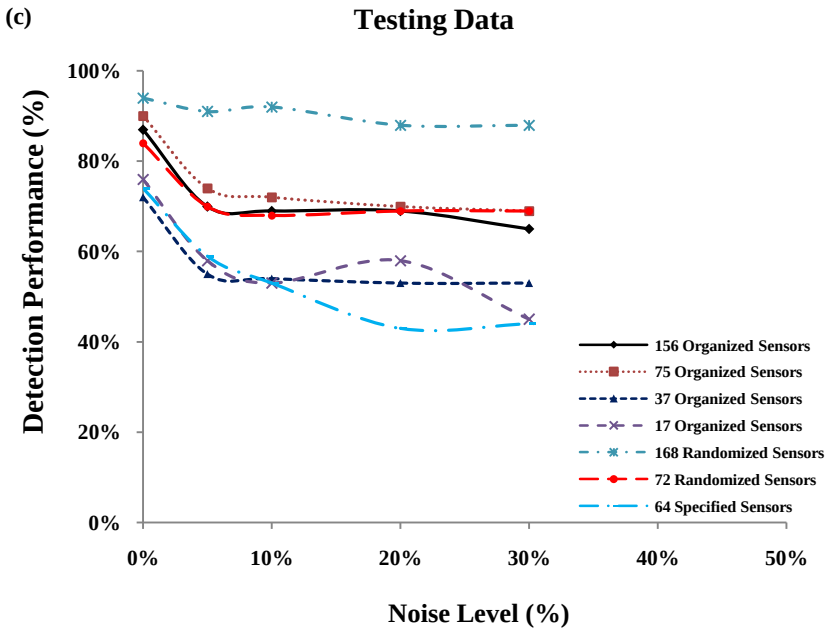

Fig. 22. The damage detection accuracy of the best models versus the noise levels for different number of sensors

5. Discussion and Conclusions

The present study proposes a new approach for the structural damage detection based on the simulation of the SWS data. New strategies are defined to interpret the limited data provided by the SWS. A probabilistic method is combined with FE to analyze the cumulative time distributions at preselected discrete strain levels. Two stages are considered for the performance verification of the proposed approach. At the first stage, the method is applied to detect different damage scenarios introduced to a simply supported beam under three-point bending. Thereafter, the efficiency of the method is examined against the complicated case of bridge gusset plate. Various descriptive features are extracted from the cumulative limited compressed static strain data and then input to the PNN models. Several analyses are performed with different number of organized and randomly selected sensors. Different phases are considered to verify the generalization of the derived models. Based on the results of the beam analysis, the models developed using coordinates of the sensors, μ and σ do not provide good detection accuracy. Also, the precision of the models expectedly decreases with decreasing the number of sensors.

Thus, new predictor features (i.e., $\mu_D, \sigma_D, \mu_S, \sigma_S, Z_{\mu 1}, Z_{\sigma 1}, Z_{\mu 2}$, and $Z_{\sigma 2}$) are defined that contain the information supplied by all the sensors in each specific sensor configuration. The results indicate that the performance of the models is improved by introducing the sensor group effect, even for low number of sensors. Consequently, it is found that $\mu_D, \sigma_D, \mu_S, \sigma_S, Z_{\mu 1}, Z_{\sigma 1}, Z_{\mu 2}$, and $Z_{\sigma 2}$ contain useful information for the detection of the damage state of the investigated system. Besides, acceptable results are obtained for the case of limited number of sensors located in the mid-span of the beam and above the notch. Based on the results obtained in the first analysis stage, $Z_{\mu 1}, Z_{\sigma 1}, Z_{\mu 2}$, and $Z_{\sigma 2}$ are used for detecting damage states introduced to the gusset plate. The performance of the method for the gusset plate case is good, especially for higher number of sensors. In order to introduce uncertainty and simulate the performance of real sensors, Gaussian noise is applied to the data. Based on the noise pollution results, the performance of the models remains satisfactory even as the noise level is increased to 20%.

However, there are still some challenges that are the focus of future research:

a) The feasibility of utilization of the proposed damage detection approach for materials with plastic behavior.
b) Considering different type of damages, as well as different type of structures for the case study of damage identification. Besides, future study can be focused on performance assessment of the proposed approach for damage localization.
c) Development a process to find the optimal number of the memory cells of the wireless sensors to achieve the most appropriate strain pattern
d) Although the FE simulation results still remain the standard for most of the elasticity problems [51], verification of the proposed approach with laboratory experiments would be an interesting topic for future study.
e) The PNN algorithm utilized for damage classifications is a supervised learning method based on the labeled data. Future research may focus on detecting damage for the cases where the target classes are unknown. To this aim, unsupervised learning algorithms such as self-organizing map (SOM) seem to be the most efficient tools.

Acknowledgment

The presented work is supported by a research grant from the Federal Highway Administration (FHWA) (DTFH61-13-H-00009). The authors are thankful to Dr. Nicholas Brake for his constructive comments.

References

1. M. Malekzadeh, G. Atia, F. N. Catbas, Performance-based structural health monitoring through an innovative hybrid data interpretation framework. J Civil Struct Health Monit 5.3 (2015) 287-305.
2. M. Malekzadeh, M. Gul, I.B. Kwon, F. N. Catbas, An integrated approach for structural health monitoring using an in-house built fiber optic system and non-parametric data analysis. Smart Struct Syst 14 (2014) 917-942
3. J.J. Lee, J.W., Lee J.H. Yi, C.B. Yun, H.Y. Jung, Neural networks-based damage detection for bridges considering errors in baseline finite element models. J. Sound Vibr. 280 (2005) 555–578
4. S. Shang, G.J. Yun, B.R. Kim, H.K. Lee,). Parameter estimation of a rate-dependent damage constitutive model for damage-tolerant brittle composites by Self-OPTIM analyses. International Journal of Damage Mechanics (2012), doi: 10.1177/1056789512464634.
5. S.W. Doebling, C.R. Farrar, M.B. Prime, D.W. Shevitz, Damage Identification and Health Monitoring of Structural and Mechanical Systems from Changes in Their Vibration Characteristics: A Literature Review, Technical Report LA-13070-MS, Los Alamos National Laboratory, NM (1996).
6. Y. Zou, L. Tong, G.P. Steven, Vibration-based model-dependent damage (delamination) identification and health monitoring for composite structures—a review, J. Sound Vibr. 230 (2) (2000) 357–378.

7. N.E. Huang, Z. Shen, S.R. Long, A new view of nonlinear water waves: the Hilbert spectrum, Annual Review of Fluid Mechanics 31 (1999) 417–475.
8. Z. Hou, M. Noori, R.S. Amand, Wavelet-based approach for structural damage detection,American Society ofCivil Engineers, J. Eng. Mech. 126 (7) (2000) 677–683.
9. S.T. Quek, Q. Wang, L. Zhang, K.H. Ong, Practical issues in the detection of damage inbeams using wavelets, Smart Mater. Struct. 10 (2001) 1009–1017.
10. Z.Y. Shi, S.S. Law, L.M. Zhang, Structural damage localization from modal strain energy change, J. Sound Vibr. 218 (5) (1998) 825–844.
11. K.A. Stetson, I.R. Harrison, Redesign of structural vibration modes by finite element inverse perturbation,American Society of Mechanical Engineers, J. Eng. Power 103 (1981) 319–325.
12. C.B. Yun, K.S. Hong, Damage assessment of structures by inverse modal perturbation method, Proceedings of the4th East Asia-Pacific Conference on Structural Engineering and Construction, Seoul, Korea, (1992).
13. J.M.W. Brownjohn, P.Q. Xia, H. Hao, Y. Xia, Civil structure condition assessment by FE model updating: methodology and case studies, Finite Elements in Analysis and Design 37 (2001) 761–775.
14. C. R. Farrar, G. Park, D.W. Allen, M. Todd, Sensor Network Paradigms for Structural Health Monitoring," Struc. Ctrl. Health Mon. 13(2006) 210-255
15. H. Sohn, C. R. Farrar, F. M. Hemez, J. J. Czarnecki, D. D. Shunk, D. W. Stinemates, B. R. Nadler, A Review of Structural Health Monitoring Literature: 1996–2001," Report Number LA-13976-MS, Los Alamos National Laboratory, Los Alamos, NM (2004).
16. C. R. Farrar, Historical Overview of Structural Health Monitoring," Lecture Notes on Structural Health Monitoring Using Statistical Pattern Recognition, Los Alamos Dynamics, Los Alamos, NM (2001).
17. W. Fan, P. Qiao, Vibration-based damage identification methods: a review and comparative study. Struct. Health Monit. 10 (1) (2011) 83–111

18. Z.H. Zong, T.L. Wang, D.Z. Huang, State-of-the-art Report of Bridge Health Monitoring, Journal of Fuzhou University (Natural Science), 30 (2002) 127–152.
19. Sanayei, M., Phelps, J.E., Sipple, J.D., Bell, E.S., and Brenner, B.R. (2012). "Instrumentation, nondestructive testing, and FEM updating for bridge evaluation using strain measurements." Journal of Bridge Engineering. Vol. 17, No. 1, January/February 2012, pp. 130-138
20. Santini-Bell, E., Sanayei, M., Brenner, B., Sipple, J. and Blanchard, A., 2008. "Nondestructive Testing for Design Verification of Boston's Central Artery Underpinning Frames and Connections,"Bridge Structures, 4(2), Jun. 2008, pp. 87-98.
21. B.A. Sundaram, K. Ravisankar, R. Senthil, S. Parivalla, Wireless sensors for structural health monitoring and damage detection techniques. Current Sci. 104(11) (2013) 1496-1505.
22. Lynch, J. P., 2004, "Overview of Wireless Sensors for Real-time Health Monitoring of Civil Structures," in Proceedings of the 4th International Workshop on Structural Control, New York, NY, June 10–11, 189–194.
23. Lynch, J. P., 2005, "Design of a Wireless Active Sensing Unit for Localized Structural Health Monitoring," Journal of Structural Control and Health Monitoring, Vol. 12, No. 3–4, 405–423.
24. Lynch, J. P., Sundararajan, A., Law, K. H., Kiremidjian, A. S., Kenny, T., and Carryer, E., 2003d, "Embedment of Structural Monitoring Algorithms in a Wireless Sensing Unit," Journal of Structural Engineering and Mechanics, Vol. 15, No. 3, 285–297.
25. Lynch, J. P., Sundararajan, A., Law, K. H., Carryer, E., Farrar, C. R., Sohn, H., Allen, D. W., Nadler, B., and Wait, J. R., 2004, "Design and Performance Validation of a Wireless Sensing Unit for Structural Health Monitoring Applications," Structural Engineering and Mechanics, Vol. 17, No. 3, 393–408.
26. Kurata, M., Kim, J., Lynch, J. P., van der Linden, G. W., Seddat, H., Thometz, E., Hipley, P., Sheng, L. H (2013). "Internet-enabled Wireless Structural Monitoring Systems:

Development and Permanent Deployment at the New Carquinez Suspension Bridge," Journal of Structural Engineering, ASCE, 139(10): 1688-1702.

27. Spencer, B. F. Jr., Ruiz-Sandoval, M. E., and Kurata, N., 2004, "Smart Sensing Technology: Opportunities and Challenges," Journal of Structural Control and Health Monitoring, Vol. 11, No. 4, 349– 368.
28. Spencer, B. F. Jr., 2003, "Opportunities and Challenges for Smart Sensing Technology," in Proceedings of the International Conference on Structural Health Monitoring and Intelligent Infrastructure, Tokyo, Japan, November 13–15, Vol. 1, 65–71.
29. Yonghui A, Spencer, B. F. Jr., Jinping O. (2015) A Test Method for Damage Diagnosis of Suspension Bridge Suspender Cables. Computer-Aided Civil and Infrastructure Engineering, DOI: 10.1111/mice.12144
30. Zou Z., Bao Y., Li H., Spencer, B. F. Jr., Embedding Compressive Sensing-Based Data Loss Recovery Algorithm Into Wireless Smart Sensors for Structural Health Monitoring. Sensors Journal, IEEE, 15(2), 797 - 808.
31. D.G. Watters, P. Jayaweera, A.J. Bahr, D.L. Huestis, N. Priyantha, R. Meline, R. Reis, D. Parks, Smart Pebble: Wireless Sensors for Structural Health Monitoring of Bridge Decks', Proceedings of SPIE (2003) 5057 20-8.
32. J.P. Lynch, K.J. Loh, A summary review of wireless sensors and sensor networks for structural health monitoring', Shock and Vibration Digest 38 (2006) 91-128,
33. S. Cho, C. Yun, J.P. Lynch, A.T. Zimmerman, B.F.Jr Spencer, T. Nagayama, Smart wireless sensor technology for structural health monitoring of civil structures', Int. J. Steel Struct. 8 (2008) 267–75.
34. M.J. Chae, H.S. Yoo, J.Y. Kim, M.Y. Cho, Development of a wireless sensor network system for suspension bridge health monitoring. Autom. Constr. 21(2012) 237-252.
35. S.C. Bae, W.S. Jang, S. Woo, D.H. Shin, Prediction of WSN placement for bridge health monitoring based on material characteristics. Autom. Constr. 35(2013) 18-27.

36. C.B. Yun, J. Min, Smart Sensing, Monitoring, and Damage Detection for Civil Infrastructures. KSCE J Civil Eng. (2011) 15(1):1-14.
37. J. Sirohi, I. Chopra, Fundamental Understanding of Piezoelectric Strain Sensors', J. Intell. Mater. Syst. Struct., 11(2001) 246 – 257.
38. S. Roundy, P.K. Wright, J. Rabaey, A Study of Low Level Vibrations as a Power Source for Wireless Sensor Nodes', Computer Communications 26 (2002) 1131-1144.
39. M. Rahimi, H. Shah, G.S. Sukhatme, J. Heideman, D. Estrin, Studying the Feasibility of Energy Harvesting in a Mobile Sensor Network', Proceedings of the 2003 IEEE International Conference on Robotics & Automation, Taipei. Taiwan, September 14- 19, (2003) pp. 19-24.
40. N. Lajnef, W. Borchani, R. Burgueño, S. Chakrabartty (2014), Self-powered Piezo-Floating-Gate Smart-Gauges based on Quasi-static Mechanical Energy Concentrators and Triggers, IEEE Sensors Journal, 15 676-683 DOI: 10.1109/JSEN.2014.2351398..
41. N. Lajnef, R. Burgueño, W. Borchani, Y. Sun (2014), "A Concept for Energy Harvesting from Quasi-static Structural Deformations through Axially Loaded Bilaterally Constrained Columns with Multiple Bifurcation Points", Smart Materials and Structures, 23 055005 doi:10.1088/0964-1726/23/5/055005.
42. W. Borchani, N. Lajnef, R. Burgueño (2014), "Model development for Dynamic Energy Conversion in post-buckled multi-stable slender columns", ", ASME Conference on Smart Materials, Adaptive Structures and Intelligent Systems, Newport, Rhode Island, September 2014.
43. N. Lajnef, W. Borchani, R. Burgueno, and S. Chakrabartty, "Energy Concentrators for Piezo-powered Quasi-static Data Logging", proceedings of the 6th World Conference on Structural Control and Monitoring (6WCSCM), Barcelona, Spain, July 2014.
44. W. Borchani, N. Lajnef, R. Burgueño (2014), "Dynamic Transitions in Multiple Bifurcation Points Mechanical Energy Concentrators", 17th U.S. National Congress on Theoretical and Applied Mechanics, Michigan State University, June 2014.

45. N. Lajnef, R. Burgueno, W. Borchani, S. Chakrabartty (2014), “Sub-Hz Self-Powered Sensing Based on Mechanical-Buckling Driven Hot-Electron Injection”, International Symposium on Circuits and Systems, Melbourne, Australia, June 2014.
46. N. Lajnef, S. Chakrabartty, R. Burgueño, W. Borchani, (2014)“Quasi-static self-powered sensing and data logging”, in Proc. SPIE Sensors and Smart Structures Technologies for Civil, Mechanical, and Aerospace Systems, San Diego, USA, March 2014
47. W. Borchani, N. Lajnef, R. Burgueño (2013), “Control of Snap-through Transitions in the Response of Mechanically-equivalent Frequency Modulators”, ASME Conference on Smart Materials, Adaptive Structures and Intelligent Systems, Snowbird, UT, September 2013.
48. N. Lajnef, R. Burgueño, S. Chakrabartty, W. Borchani (2013),“Self-powered Sensing System for the Monitoring of Quasi-static Structural Response”, ASME Conference on Smart Materials, Adaptive Structures and Intelligent Systems, Snowbird, UT, September 2013.
49. H. Salehi, T. Taghikhany, A Y. Fallah, Seismic protection of vulnerable equipment with semi-active control by employing robust and clipped-optimal algorithms. Int J Civil Eng 12 (4), (2014) 413-428.
50. N. Elvin, A. Elvin, M. Spector, A self-powered mechanical strain energy sensor. Smart Mater. Struct. 10 (2001) 293–299.
51. N. Elvin, A. Elvin, Choi D. H., A self-powered damage detection sensor", J. Strain Anal. 38(2) (2003) 115 -124.
52. N. Lajnef, M. Rhimi, K. Chatti, L. Mhamdi, Toward an Integrated Smart Sensing System and Data Interpretation Techniques for Pavement Fatigue Monitoring. Comput.-Aided Civ. Infrastruct. Eng. 26(2011) 513–523.
53. N. Lajnef, S. Chakrabartty, N. Elvin, A Piezo-powered Floating-gate Sensor Array for Long-term Fatigue Monitoring in Biomechanical Implants, IEEE Trans. Biomed. Circuits Syst. 2(3) (2008) 164-172.

54. N. Lajnef, K. Chatti, S. Chakrabartty, M. Rhimi, P. Sarkar, Smart Pavement Monitoring System". Report: FHWA-HRT-12-072, Federal Highway Administration (FHWA), Washington, DC (2013).
55. C. Huang, N. Lajnef, S. Chakrabartty, Self-calibration and characterization of self-powered floating-gate usage monitors with single electron per second operational limit, IEEE Trans. Biomed. Circuits Syst. I, 57 (2010) 556-567.
56. A. Tessler, H. R. Riggs, C.E. Freese , G. M. Cook, An improved variational method for finite element stress recovery and a posteriori error estimation, Comp. Meth. Appl. Mech. Eng. 155(2) (1998) 15–30.
57. A. P. Dempster, , N. M. Laird, D. B. Rubin, Maximum likelihood from incomplete data via the EM algorithm, J. Royal Statistical Society B-39(1) (1977) 1–38.
58. Goh A.T.C., Probabilistic neural network for evaluating seismic liquefaction potential, Can. Geotech. J., 39,pp.219-232, 2002.
59. N.G. Singh, M. Joshi, Optimization of location and number of sensors for structural health monitoring using genetic algorithm, Mater Forum 33(2009) 359-67.
60. C. Huang, S. Chakrabartty, An Asynchronous Analog Self-powered Sensor-Data-Logger with a 13.56MHz RF Programming Interface", IEEE Journal of Solid-State Circuits, 47(2012) DOI:10.1109/JSSC.2011.2172159.
61. N. Elvin, C. K. Y. Leung, A fast iterative boundary element technique for solving closed crack problems. Engng Fracture Mechanics 63(5) (1999) 631-650.
62. Rosenstrauch, P.L., Sanayei, M., and Brenner, B.R., 2013. "Capacity Analysis of Gusset Plate Connections Using the Whitmore, Block Shear, Global Section Shear, and Finite Element Methods," Engineering Structures, Vol. 48, March 2013
63. Jesse D. Sipple and Masoud Sanayei, 2013. "Finite Element Model Updating Using Frequency Response Functions and Numerical Sensitivities", 2013. Structural Control and Health Monitoring, September 2013.

64. NTSB, Structural and local failure study of gusset plate in minneapolis bridge collapse. Report - NTSBC070010, National Transportation Safety Board (NTSB), Washington, DC (2008).
65. M. Liao, T. Okazaki, R. Ballarini, A.E. Schultz, T.V. Galambos, Nonlinear Finite-Element Analysis of Critical Gusset Plates in the I-35W Bridge in Minnesota. J. Struct. Eng. ASCE, (2011) 59-69.
66. M. Liao, T. Okazaki, A Computational Study of the I-35W Bridge Collapse. Final Report, CTS Project # 2008049, Center for Transportation Studies, University of Minnesota, Minneapolis, MN (2009).
67. R. Holt, J. Hartmann, Adequacy of the U10 & L11 Gusset Plate Designs for the Minnesota Bridge No. 9340 (I-35 over the Mississippi River) Interim Report, Federal Highway Administration, (2008).
68. S. Hao, I-35W Bridge Collapse. J. Bridge Eng. ASCE (2010) 608- 614.
69. N. Moes, J. Dolbow, T. Belytschko, A finite element method for crack growth without remeshing, Int. J. Numer. Methods Eng. 46 (1) (1999) 131–150.
70. I. Flood, P. Christophilos, Modeling construction processes using artificial neural networks. Autom. Constr. 4(4) (1996) 307-320.
71. N. Kartam, I. Flood, Construction simulation using parallel computing environments. Autom. Constr. 10(1) (2000) 69-78.
72. M. A. Shahin, M. B. Jaksa, Neural network prediction of pullout capacity of marquee ground anchors, Computers and Geotechnics, 32(3) (2005) 153-163.
73. S.K. Das, P.K. Basudhar, Prediction of Residual Friction Angle of Clays Using Artifical Neural Network. Eng Geol 100(3-4) (2008) 142–145
74. P. Samui, Support vector machine applied to settlement of shallow foundations on cohesionless soils. Computers and Geotechnics 35 (3) (2008) 419-427.
75. M.A. Shahin, Intelligent computing for modelling axial capacity of pile foundations, Canadian Geotechnical Journal, 47(2) (2010) 230-243.

76. A.H. Gandomi, A.H. Alavi, M.G. Sahab, New formulation for compressive strength of CFRP confined concrete cylinders using linear genetic programming. Materials and Structures 43(7) (2010) 963–983.
77. S.K. Das, P. Samui, A.K. Sabat, T.G. Sitharam Prediction of swelling pressure of soil using artificial intelligence techniques. Environ Earth Sci 61(2) (2010) 393-403
78. A.H. Alavi, A.H. Gandomi, Prediction of Principal Ground-Motion Parameters Using a Hybrid Method Coupling Artificial Neural Networks and Simulated Annealing, Comput. Struct. 89 (23-24) (2011) 2176-2194.
79. A.H. Alavi, A.H. Gandomi A Robust Data Mining Approach for Formulation of Geotechnical Engineering Systems. Engineering Computations 28(3) (2011) 242-74.
80. S.K. Das, P. Samui, A.K. Sabat, Application of Artificial Intelligence to Maximum Dry Density and Unconfined Compressive Strength of Cement Stabilized Soil. Geotech Geol Engi 29(3) (2011) 329-342
81. S.K. Das, P. Samui, S.Z. Khan, N. Sivakugan, Machine learning techniques applied to prediction of residual strength of clay. Cent Europ J Geosci 3(4) (2011) 449-461.
82. H.M. Azamathulla, A. Guven, Y.K. Demir, Linear genetic programming to scour below submerged pipeline. Ocean Eng 38(8–9) (2011) 995-1000.
83. H.M. Azamathulla, F.C. Wu, Support vector machine approach for longitudinal dispersion coefficients in natural streams. Appl Soft Comput 11(2) (2011) 2902-2905.
84. P. Samui, Application of statistical learning algorithms to ultimate bearing capacity of shallow foundation on cohesionless soil. Int. J. Num. Anal. Meth. Geomech. 36(1) (2012) 100–110.
85. H.M. Azamathulla, Gene expression programming for prediction of scour depth downstream of sills. J Hydrol 460–461 (2012) 156-159.
86. H. Salehi., S. Das, , S. Chakrabartty, Biswas, R. Burgueno, Structural assessment and damage identification algorithms using binary data: ASME 2015 conference on smart

materials, adaptive structures and intelligent systems (SMASIS2015), Colorado Springs, Colorado, 2015.

87. S.K. Babanajad, A.H. Gandomi, D. Mohammadzadeh, A.H. Alavi, Numerical modeling of concrete strength under multiaxial confinement pressures using linear genetic programming. Autom. Constr., 36(2013) 136-144.
88. M.Y. Cheng, M.T. Cao, D.H. Tran, A hybrid fuzzy inference model based on RBFNN and artificial bee colony for predicting the uplift capacity of suction caissons. Autom. Constr., 41(2014) 60-69.
89. M.S.El-Abbasy, A. Senouci, T. Zayed, F. Mirahadi, L. Parvizsedghy, Artificial neural network models for predicting condition of offshore oil and gas pipelines. Autom. Constr., 45(2014), 50-65.
90. J.S. Chou, A.D. Pham, Hybrid computational model for predicting bridge scour depth near piers and abutments. Autom. Constr., 48(2014) 88-96.
91. R.S. Adhikari, O. Moselhi, A Bagchi. Image-based retrieval of concrete crack properties for bridge inspection. Autom. Constr., 39(2014) 180-194.
92. M. A. Shahin, Load-settlement modeling of axially loaded steel driven piles using CPT-based recurrent neural networks, Soils and Foundations, 54(3) (2014) 515-522.
93. M. A. Shahin, Use of evolutionary computing for modelling some complex problems in geotechnical engineering, Geomechanics and Geoengineering: An International Journal, (2014) 1-17.
94. P. Yuvaraj, A.R. Murthy, N.R. Iyer, P. Samui, S.K. Sekar, Prediction of fracture characteristics of high strength and ultra high strength concrete beams based on relevance vector machine. International Journal of Damage Mechanics (2014) 1056789514520796.
95. P. Szewezyk, P. Hajela, Damage detection in structures based on feature - sensitive neural networks. J. Comp. Civ. Engrg. ASCE 8(2) (1994) 163 - 178.
96. X. Wu, J. Gahboussi, J.H. Garrett, Use of neural networks in detection of structural damage[J] . Comput. Struct. 42(4) (1992) 649 - 659.

97. S.F. Masri, A.G Chassiakos, T.K. Caughey, Identification of nonlinear dynamic systems using neural networks . J.Appl. Mech. Trans. ASME 60 (1993) 123 - 133.

98. M.F Elkordy, K.C. Chang, G.C. Lee, Neural networks trained by analytically simulated damage states. Journal of Comp in Civ Engrg , ASCE 7(2) (1993) 130 - 145.

99. R.I. Levin, N.A.J. Lieven, Dynamic finite element model updating using neural network[J] . J. Sound Vibr. 210 (5) (1998) 593 - 607.

100. J. Zhao, J.N. Ivan, J.T. DeWolf, Structural Damage Detection Using Artificial Neural Networks, J. Infrastruct. Syst. ASCE, 4(3) (1998) 0093-0101.

101. T. Marwala, Damage identification using committee of neural networks[J]. J. Engrg Mech , ASCE 126(1) (2000) 43 - 50

102. C.C. Chang, T.Y.P., Chang, Y.G. Xu, M.L. Wang, Structural damage detection using an iterative neural network." J. Intelligent Mater. Syst. Struct. 11(2000) 32-42.

103. C. Zang, M. Imregun, Structural damage detection using artificial neural networks and measured FRF data reduced via principal comoponent projection. J. Sound Vibr. 242(5) (2001) 813 - 827.

104. H. Adeli, X. Jiang, Dynamic fussy wavelet neural network model for structural system identification. J.Struct. Eng. 132(2006) 102-111.

105. S. J. S. Hakim, H. Abdul Razak, Structural damage detection of steel bridge girder using artificial neural networks and finite element models. Steel Compos. Struct. 14(2013) 367-377.

106. B. Yan, A. Miyamoto, Application of probabilistic neural network and static test data to the classification of bridge damage patterns," Smart Structures and Materials 2003: Smart Systems and Nondestructive Evaluation for Civil Infrastructures, Liu, Shih-Chi. Proceedings of the SPIE (2003) 5057, 606-617.

107. D. Specht, Probabilistic Neural Networks. Neural Networks 3(1990) 109-118.

108. B.A. Mogan, Damage Detection and Localization using Probabilistic Neural Networks, Research Conducted at Keio University Tokyo, Japan, (2005).

109. J.J. Lee, C.B. Yun, Damage localization for bridges using probabilistic neural networks." KSCE J. Civil Eng. 11 (2007) 111–120.

110. M.P. Paulraj, Y, Sazali, M.S. Abdul, K. Pranesh, Steel Plate Damage Diagnosis Using Probabilistic Neural Network. 7th International Conference on Intelligent Systems and Control (ISCO), (2013) 545 - 549.

111. V. Giurgiutiu, C. Kropas-Hughes, Comparative study of neural-network damage detection from a statistical set of electro-mechanical impedance spectra, SPIE's 10th annual international symposium on smart structures and materials and 8th annual international symposium for on NDE for health monitoring and diagnostics, San Diego (2002) 1 – 12.

112. S.E. Klenke, ad T.L. Paez, Damage identification with probabilistic neural networks. Proceedings of the 14th International Modal Analysis Conference, pages 99-104, (1996).

113. Y.Q. Ni, S.F. Jiang, J.M. Ko, Application of adaptive probabilistic neural network to damage detection of Tsing Ma suspension bridge, Proc. SPIE 4337, Health Monitoring and Management of Civil Infrastructure Systems, 347 (2001); doi:10.1117/12.435610.

114. H. Adeli, A. Panakkat, A probabilistic neural network for earthquake magnitude prediction. Neural Networks 22 (2009) 1018-1024.

115. A. H. Alavi, M. Ameri, A. H. Gandomi, M. R. Mirzahosseini, Formulation of flow number of asphalt mixes using a hybrid computational method. Constr. Build. Mater. 25(3) (2011) 1338-1355.

116. R. Kohavi, P. Foster, Glossary of terms, Machine Learning 30 (1998) 271-274.

117. S.F. Jiang, C. Fu, C. Zhang, A hybrid data-fusion system using modal data and probabilistic neural network for damage detection. Adv. Eng. Soft. 42(2011) 368–374